Chemical Science

Accepted Manuscript

This article can be cited before page numbers have been issued, to do this please use: C. Atienza, F. García and L. Sanchez, *Chem. Sci.*, 2026, DOI: 10.1039/D6SC00729E.

ROYAL SOCIETY OF CHEMISTRY

rsc.li/chemical-science

ARTICLE Journal Name

CPL-active supramolecular polymers

View Article Online
DOI: 10.1039/D6SC00729E

Carmen Atienza,[a] Fátima García[a] and Luis Sánchez*[a]

Received 00th January 20xx,
Accepted 00th January 20xx

DOI: 10.1039/x0xx00000x

Supramolecular polymers constitute a highly dynamic and rapidly evolving research field, characterized by the continuous development of systems with increasing structural and functional complexity. Theoretical and mathematical models aimed at understanding the mechanisms of supramolecular polymer formation have played a crucial role in guiding the design of these systems, enabling the discovery of novel assembly pathways and emergent functionalities in both self- and co-assembled architectures. Within this broad landscape, chiral supramolecular polymers occupy a particularly prominent position, as they provide an effective platform for generating well-defined helical structures that can serve as models for the emergence of homochirality in nature, while simultaneously enabling a wide range of advanced functional properties. Of particular interest is the incorporation of emissive moieties into the monomeric building blocks of chiral supramolecular polymers, which can lead to the formation of emissive aggregated species exhibiting circularly polarized luminescence (CPL). The CPL activity of these systems significantly enhances their relevance across multiple research areas, extending their impact beyond fundamental supramolecular chemistry to applied materials science. This review focuses on representative examples of the diverse strategies employed to obtain CPL-active supramolecular polymers, including the introduction of chiral elements—such as point or axial chirality—into monomeric units, as well as the integration of metallic components. Furthermore, the collected examples demonstrate the high responsiveness of CPL-active supramolecular polymers to external stimuli such as light, solvent polarity and temperature, highlighting their exceptional versatility. These adaptive properties enable the realization of systems with notably high dissymmetry factors (g_{lum}) and circularly polarized luminescence brightness (B_{CPL}). Finally, the review presents both metallo-organic and purely organic CPL-active supramolecular polymers, together with selected examples of their outstanding applications in areas such as optoelectronic devices, anticounterfeiting technologies, and information encryption.

Introduction

Supramolecular polymers (SPs) are those in which discrete molecules –named as monomers– are held together by non-covalent interactions.[1] First reports on supramolecular polymers date back early 1990s from Aida, Lehn and Meijer.[2] The dynamic nature of these interactions on which supramolecular polymers are constructed, can yield to interesting applications in which responsiveness is required, such as adhesives, self-healing materials, drug delivery, optoelectronics or catalysis.[3] Interestingly, the functionalization of the monomeric species with elements of asymmetry allows achieving chiral supramolecular polymers.[4] It is worth mentioning that chirality is a geometric property exhibited by a number of chemical compounds, which can be chiral if they cannot be superimposed on their mirror image. The most common, but not the only one, type of chirality in single molecules comes from the existence of four different substituents on a tetrahedral atom, named as stereogenic centre, such as a sp^3 carbon, which can be geometrically arranged in two ways, giving rise to a pair of enantiomers. Enantiomers may exhibit different chemical properties of special interest in areas such as chemical biology, medicinal chemistry, etc. At the molecular level, there are different chirality sources: point chirality, which corresponds to the asymmetry originated by the presence of stereogenic centres, or axial and helical chirality, where a molecule does not possess a stereocenter (like a chiral carbon) but instead features an axis of chirality as occurs for instance in allenes, binaphthyls or helicenes (Figure 1a). Chirality can also exist at the supramolecular level, for example in helical supramolecular polymers that can be right or left-handed, depending on the chiral motifs present at the monomeric structure. It can happen that the formation of one-sided helix can be energetically favoured and, therefore, formed in excess towards the opposite one.[4]

It is well-known that light is an electromagnetic wave, and the electric field of this wave oscillates perpendicularly to the direction of propagation. In sunlight, the direction of the electric field randomly fluctuates in time and, therefore, it is unpolarized. But, on the other hand, if the direction of the electric field is confined to a certain plane or direction along the propagation direction, the light is polarized. In circular polarized electromagnetic radiation, the electric field vector is comprised of two perpendicular components of equal magnitude 90°. This results in a rotation of the electric field vector around the propagation direction in time forming a helix which can be right (RCP light) or left-handed (LCP light), yielding what can be called chiral light (Figure 1b). Chiral molecules can absorb differently RCP or LCP light thus giving rise to circular dichroism. In analogy, chiral luminogens can emit an excess of RCP or LCP radiation which generates circular polarized luminescence (CPL). To quantify the CPL emitted by a system, the dissymmetry luminescence factor (g_{lum}) is utilized. This parameter g_{lum} defined as the ratio between the LCP and RCP light intensities (ΔI)[5] emitted and the average intensity (I_0) (Eq. 1). The g_{lum} expresses the extension of CPL emitted of a system and its maximum value can vary from values of -2 to +2, indicating a 100% of RCP and LCP emission, respectively.[6]

[a] Prof. Dr. C. Atienza, Prof. Dr. F. García, Prof. Dr. L. Sánchez.
Departamento de Química Orgánica; Facultad de Ciencias Químicas
Universidad Complutense de Madrid Ciudad Universitaria s/n; 28040-Madrid (Spain) E-mail: lusamar@ucm.es

† Footnotes relating to the title and/or authors should appear here.

$$g_{lum} = \frac{\Delta I}{I_0} = \frac{I_L - I_R}{\frac{1}{2}(I_L + I_R)} \quad (1)$$

Theoretically, in an isotropic medium, $g_{lum}$is related with the magnetic (m) and electric (n) dipole moments, and the angle between them (θ) by Eq. 2.

$$g_{lum} = 4cos\theta \frac{|m| \cdot |n|}{|m|^2 + |n|^2} \quad (2)$$

By analysing Eq. 2 it can be concluded that there are main strategies to attain high values of the dissymmetry luminescence factor and, therefore, the performance of a CPL emitter. Firstly, the variation of the angle between the magnetic and the dipole moments affects g_{lum} values. When both vectors are parallel or antiparallel ($\theta = 0°$ or $180°$) maximum $|g_{lum}|$ values ($cos\theta = 1$ or -1, respectively) are reached. Secondly, similar magnitudes of both vectors will also maximize $|g_{lum}|$. Most organic molecules exhibit low dissymmetry factors ($g_{lum} = 10^{-5}$ - 10^{-3}). In organic molecules with rigid aromatic moieties the electric dipole transitions are allowed ($\pi \rightarrow \pi^*$), leading to a difference on the m and n values in several order of magnitudes. In contrast, lanthanide-based complexes this factor ranges from 0.1 to 1 due to their forbidden electric dipole transitions (4f → 4f).[6b] However, the search for organic systems with enhanced CPL remains of significant importance, owing to their ease of processing and reduced manufacturing costs. Their dissymmetry factor has been proved to be improved when these chiral organic molecules are part of supramolecular assemblies or liquid crystals.

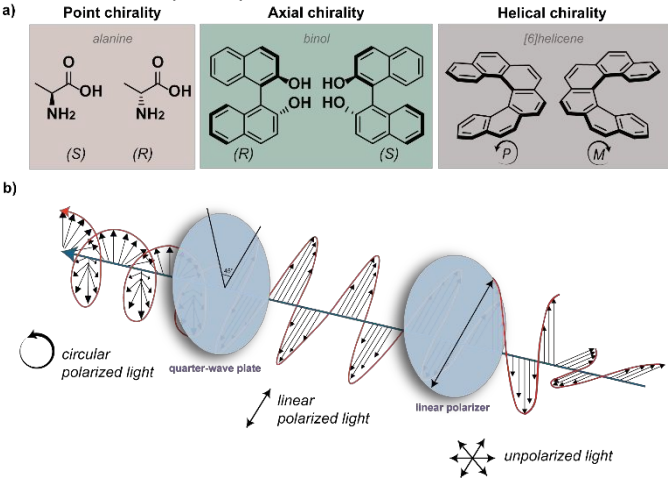

Fig. 1. (a) Examples of chiral molecules bearing different sources of chirality; (b) schematic representation of the generation of circular polarized light.

To evaluate the performance of a CPL luminogen it is not enough to evaluate the dissymmetry factor as it only considers the relative excess of one-handed light emitted but not considering the total number of circularly polarized photons emitted by the fluorophore. For this purpose, the CPL brightness (B_{CPL}) is a parameter with can serve to compare the performance of different CPL fluorophores as includes the quantum yield (ϕ), which is the ratio between the number of photons emitted from the photons absorbed, the molar extinction coefficient (ε_λ) measured at the excitation wavelength (λ) and the absolute value of the g_{lum}(Eq. 3).

View Article Online DOI: 10.1039/D6SC00729E

$$B_{CPL} = \frac{1}{2}\varepsilon_\lambda \cdot \phi \cdot |g_{lum}| \quad (3)$$

Since the B_{CPL} parameter can only serve for samples in solution, Zinna et al. suggested to use the parameter B'_{CPL} for calculating the CPL brightness for solid-state samples (Eq. 4), in analogy with the more general brightness parameter B', which can serve for aggregated, supramolecular and solid-state sample luminogens; where ε_{abs} is the absorption efficiency measurable with an integrating sphere.[7]

$$B'_{CPL} = \frac{1}{2}\varepsilon_{abs} \cdot \phi \cdot |g_{lum}| \quad (4)$$

The first report on a CPL-active organic compound dates to 1967 for a bicyclic chiral ketone.[8] Since then, numerous reports on organic and metalloorganic compounds and metal centres have been described to behave as CPL emitters.[9]

General strategies to obtain materials with elevated CPL efficiency combine a luminescence motif (chiral or not), which can be organic or a metallic centre, with a chiral component (e.g. point, axial or helicoidal) and both components should be electronically coupled in a covalent or non-covalent manner. For non-covalent strategies, and in particular for CPL-emissive supramolecular polymers, the responsible of the efficient luminescence can be a metal ion, or an aggregate induce emission (AIE) motif.[10] Supramolecular polymers presenting high dissymmetry factors, as well as covalent polymers, present lower production costs than lanthanide complexes which are scarce and highly pure samples are needed; both factors contribute to increase production costs. Also, SPs can be designed with a variety of non-covalent interactions providing wider structural diversity in comparison with liquid crystals. Advantages of supramolecular polymers over covalent polymers for CPL materials are related with their dynamic nature and therefore, the CPL emission can be switched on/off upon external stimuli.[11] As a sum, the search of supramolecular polymers as efficient CPL emitters is a hot topic in the area.

A key issue in the field of supramolecular polymers is the mechanism governing the formation of such organized supramolecular entities. There are mainly two types of supramolecular polymerization mechanisms: isodesmic and cooperative or nucleation-elongation. In the isodesmic mechanism, the addition of each monomer to the polymer chain, regardless its length, occurs with the same equilibrium constant. In contrast, in the cooperative mechanism, the initial formation of a nucleus is needed. This process is described by a nucleation constant (K_n). After that, the addition of more monomers to the nuclei to give rise the polymer chain takes place. This second process is described by an elongation constant (K_e) and it is thermodynamically favoured in comparison to the nucleation ($K_e > K_n$). The difference between both mechanisms has implications in the final properties of the SPs. Thus, isodesmic SPs are more polydisperse and have lower

degree of polymerization than cooperative SPs.[1] When point, axial or helical chiral motifs are included in the chemical structure of the monomeric species an efficient transfer of asymmetry yields chiral SPs. In addition, the formation of chiral SPs can be achieved by an amplification of asymmetry process in which a mixture of two or more monomeric species is utilized. Two different strategies can be utilized to achieve an amplification of asymmetry: i) the Sergeants-and-Soldiers, in which a mixture of an achiral monomeric species and a chiral congener present the same handedness to that of the pristine chiral system, and ii) Majority Rules, in which a mixture of two enantiomer at different ratio obliges to the enantiomer in less ratio to adopt the handedness of the monomer in excess.[4] In any case, the transfer of amplification of asymmetry can yield *M*- or *P*-type helical SPs showing with high dissymmetry factor values if a strong exciton coupling operates. Another important aspect of supramolecular polymerization is pathway complexity, in which the same monomer can lead to different types of aggregates which can be formed following a consecutive or a competitive regime. In the consecutive process one aggregate is formed first and then serves as template of the next one, leading to hierarchical organization. In the competitive process one aggregate must disassemble prior to form the other aggregate type and therefore, the molecular assembly in both aggregates does not need to relate to each other. In terms of the CPL, different aggregates can show differences in the CPL, such as wavelength, dissymmetry factors, and/or sign. Noteworthy, an emerging concept to attain higher-order aggregates is secondary nucleation,[12] a strategy that has been recently demonstrated as an efficient strategy to achieve efficient CPL-active supramolecular polymers.[13]

In the field of CPL-active materials, it should be mentioned that a careful inspection of large g_{lum} values for supramolecular gels and solids must be taken because they can be distorted by scattering, linear dichroism (LD)/birefringence (LB), macroscopic alignment, and thickness effects. Reliable CPL measurements therefore should be accompanied of negligible LD and LB, verification that the signal is independent of sample orientation, and minimization of scattering. True CPL spectra should follow the fluorescence profile and remain unchanged with path length in the non-reabsorbing regime. Instrument calibration with achiral emitters and controls that disrupt supramolecular chirality should yield no signal. Another important issue is to assure the sample purity and optical purity. These precautions help ensure that observed CPL arises from intrinsic chiral emission rather than optical artifacts. Furthermore, a reliable comparison of different parameters related to CPL-active materials (g_{lum}, B_{CPL}) involves that they should be measured at the same wavelength and at the maximum value of emission.

In this review, we collect relevant and recent examples of CPL active supramolecular polymers, either entirely organic or metallo-organic systems, and those supramolecular polymers bearing AIE either with point, axial or helical chirality will be presented. The CPL activity shown by these chiral supramolecular polymers can be utilized for practical applications that are summarized in the last part of this review.

Although there are several reviews dealing with CPL-active materials,[6-9] the present review advances the field beyond prior publications by reframing CPL-active supramolecular polymers not merely as emissive chiral materials but as dynamic, information-rich systems whose optical activity is governed by pathway-dependent self-assembly and hierarchical organization. Whereas earlier reviews catalogue molecular designs, chiroptical performance, and applications, we provide evidence that supramolecular polymerization enables transfer and amplification of asymmetry across length scales, thereby allowing CPL to be programmed through assembly history, external stimuli, and collective behaviour. By collecting concepts such as kinetic vs thermodynamic control or living supramolecular polymerization we propose a framework in which CPL output becomes a readout of supramolecular information processing rather than a fixed molecular property. This perspective highlights underexplored opportunities—including pathway-encoded CPL states, adaptive and reconfigurable emitters—that could enable next-generation photonic materials, optical data storage, and soft matter systems with learning-like functions. By shifting the focus from structure–property correlations to process–structure–function relationships, this review aims to guide the community toward designing CPL-active SPs as programmable and organized materials, opening new directions beyond conventional molecular engineering.

CPL-active supramolecular polymers

CPL-active metallosupramolecular polymers

Chiral coordination polymers with AIE properties are attractive candidates for the design of CPL-active polymer materials. Compared with the corresponding monomeric complexes, chiral coordination polymers generally display much higher luminescence efficiencies and large $|g_{lum}|$ values. Several examples have been reported based of inorganic cluster-based AIEgens.[14] However, this section focuses on recent advances in the development of metallo-organic supramolecular polymers with tunable CPL properties, with particular emphasis on systems in which metal ions play a crucial role in controlling the assembled nanostructure and the resulting chiroptical activity. From this perspective, one of the earliest examples was reported by Liu in 2019. In this work, Liu and coworkers described a simple fluorophore based on pyrene-conjugated histidine (*L*-PyHis and *D*-PyHis, **1a**-**b**) in which the coordination with metal ions induced a switch in both the self-assembly pathways and the chirality of the resulting supramolecular systems (Figure 2a).[15] Compounds **1a**-**b** formed gels in the presence of water at room temperature, as confirmed by the rheological studies. Initially, they observed different behavior in the CD and CPL spectra of the gel and the solution states. While in gel, positive excition-type bisignated Cotton effect was observed with crossovers at 240 and 353 nm, ascribed to ^{1}Bb and ^{1}La bands of pyrene (Figure 2b), in solution the CD signal was practically null.

View Article Online DOI: 10.1039/D5SC00730E

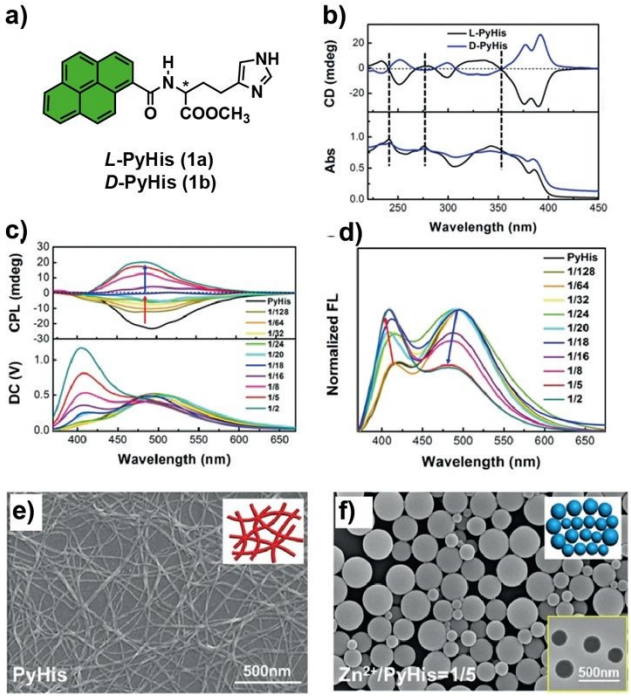

Fig. 2. (a) Chemical structure of chiral PyHis; (b) CD spectra of **1a** and **1b** gel; (c) CPL spectra and (d) fluorescence spectra change of **1a** gel in presence of different amounts of Zn^{2+}; (e) Morphology transformation detected by SEM of PyHis xero-gel; (f) SEM image of PyHis in the presence of Zn^{2+}; the inserted figure in the bottom right corner is the TEM image of the nanospheres (reprinted from reference 15 with permission from Wiley-VCH. Copyright 2019).

These CD signals suggested that the chirality localized at histidine moiety was transferred into the assemblies in the gel. In addition, mirror-image CPL signals were also obtained for **1a-b** gels with emission band centered at 500 nm, corresponding to the emission peak of the pyrene excimer. SEM and TEM images revealed the formation of nanofibers for PyHis gel (Figure 2e). However, the addition of Zn^{2+} to the PyHis gel caused a change in the morphology: The nanofibers were converted into nanospheres when the Zn^{2+}/PyHis ratio reached 1:5 or higher, as shown by SEM and TEM microscopy (Figure 2f). Moreover, these nanoparticles were chiral and emissive, too. The fluorescence spectrum showed how the increase of Zn^{2+} provoke that the peak ascribed to monomer emission at 403 nm increased while the excimer emission at 500 nm decreased simultaneously (Figure 2d). Remarkably, when increasing the ratio of Zn^{2+} the intensity of CD and CPL decreased gradually and became silent at a 1:18 ratio, and then reversed as it was continually increased, in a reversible manner (Figure 2c). The back-switching from PyHis/Zn^{2+} complex to PyHis assemblies could be realized by adding EDTA as a competing ligand. The analysis of the crystal structure by single-crystal X-ray diffraction revealed the possible mechanism of chirality switching and inversion of optical properties. The packing diagram of PyHis indicated a monoclinic structure in which two adjacent pyrene planes are almost perpendicular to each other and thus formed intermolecular CH-π interactions with dihedral angles between these two pyrene planes about 83°, this packing mode is almost identical in the gel. Furthermore, the *d*-spacing of 2.23 nm in PXRD is larger than once but shorter than twice the molecular length of PyHis (1.26 nm), which suggests that two pyrene rings form a structural unit by intermolecular CH-π interaction or T-shaped π-stacking and further self-assembled into nanofibers. While for Zn^{2+}-mediated PyHis assemblies, high-resolution mass spectroscopy (HRMS), NMR, DFT calculations confirmed the formation of a pentacoordinated complex $[(Zn\text{-}(PyHis)_5]^{2+}$, the PXRD pattern of the $[(Zn\text{-}(PyHis)_5]^{2+}$ revealed the presence of a peak at 0.35 nm which implied tight π-π stacking between pyrene units. This structural change in the dihedral angle about 90° favored the hydrogen bonding interactions between the amide functional groups and the π-stacking between the pyrene units compared with the PyHis crystals. The big change of dihedral angle between two chromophores may lead to the reversal of supramolecular chirality through different spatial arrangements and excitonic coupling interactions. These findings provide mechanistic insights into how metal incorporation induces structural reorganization, thereby altering the self-assembly pathway and causing changes in morphology and CPL response.

Multiple approaches for developing CPL-active metal-organic supramolecular polymers (MOSPs) have been reported by G. Liu *et* al,[16] in which chirality inversion can be induced by modifying the coordinated metal ions, adjusting solvent polarity, and altering assembly conditions, including ultrasonic or thermal stimuli. One of these approaches has been the MOSP pyridine-thiophene-modified cyanostilbene-cholesterol (**PTC) 2**, composed of a homochiral pyridine-cyanostilbene-cholesterol molecule that displayed multicolor CPL and chirality inversion by changing the metal ions in determined conditions (Figure 3).[16b] The chemical structure of **2** consists of a cholesterol moiety, which induced chirality, a thiophene-modified cyanostilbene unit, that promotes color-tunable aggregation induced emission (AIE), and a pyridyl moiety enabling metal coordination (Figure 3a).[16b] Initial studies showed that pyridine-cholesterol derivatives can be easily assembled into supramolecular gels under the collective influence of solvophobic effect and van der Waals forces. The gels exhibited yellow fluorescence with an emission peak around 540 nm and negative CD and CPL signals at 470-485 nm and 530 nm, respectively. The supramolecular organization was confirmed by SEM microscopy showing the presence of helical nanofibers. Another scenario arises when **2** derivatives coordinate with various metal ions. While the coordination with Fe^{2+} and Fe^{3+} promoted gel formation in addition to quenching of the emission, the addition of different metal ions such as Ag^{+}, Co^{2+}, Cu^{2+}, Mn^{2+}, Zn^{2+}, Bi^{3+} or Al^{3+} produced suspensions and Ag^{+}, Zn^{2+}, Bi^{3+} and Al^{3+} red shifted emission.

View Article Online
DOI: 10.1039/D5SC00720F

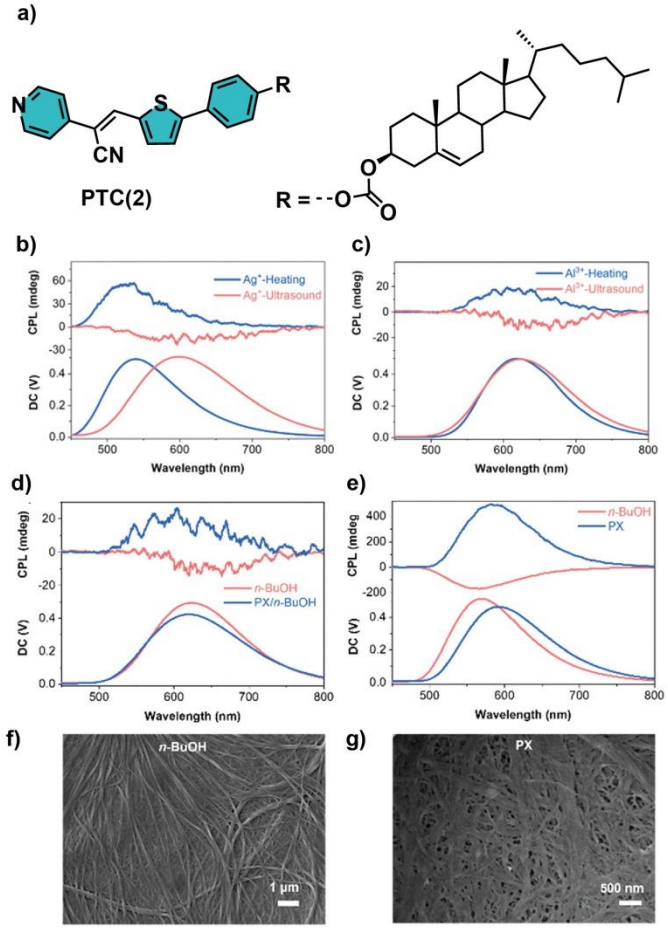

Fig. 3. (a) Chemical structure of the homochiral **PTC** (**2**); (b) CPL spectra of **2**-based MOSPs formed by adding $AgNO_3$ and (c) $AlCl_3$ in *n*-BuOH treated with ultrasound (blue line) and heating-cooling cycle (red line); (d) CPL spectra of **PTC** with $AlCl_3$ (d) and $BiCl_3$ (f) aggregates treated with ultrasound and thermally treated (e) in *n*-BuOH, PX/*n*-BuOH (v/v, 1/1) and PX, respectively; (f) SEM images of PTC + $BiCl_3$ aggregates treated with heating-cooling in *n*-BuOH and PX (g) (reprinted from reference 16b with permission from Royal Society of Chemistry. Copyright 2023).

Noteworthy were the outcomes obtained through CD studies, where the chirality inversion was induced by the change in the assembly conditions, specifically ultrasonic or thermal treatments (Figure 3b-c). Under ultrasonic conditions, **2**+Ag^+ and **2**+Al^{3+} exhibited negative CD signals and corresponding right-handed CPL at 595 and 625 nm, respectively. However, upon heating-cooling treatment, both systems display positive CD and CPL, suggesting an inversion of the supramolecular chirality. In addition, time-dependent CD monitoring indicated that ultrasonic treatment produced kinetically controlled, metastable assemblies, while thermal treatment generated thermodynamically stable structures, exhibiting cation-dependent chirality. Selective CPL studies revealed that **2**+Bi^{3+} exhibited negative CPL at 565 nm, while **2**+Zn^{2+} produced positive CPL at 560 nm, and confirmed the cation induced CPL inversion. These results indicate that coordination geometry and metal valence dictate supramolecular stacking modes and chirality outcomes. Another factor that had a significant influence on chiroptical properties was the solvent polarity (Figures 3d-e). **2**+Al^{3+} and **2**+Bi^{3+} aggregates treated with ultrasounds showed negative CD and CPL signals in polar solvents such as *n*-BuOH, however, a decrease in polarity, *p*-xylene/*n*-BuOH (1:1) and *p*-xylene (PX), caused a signal reversal in both CD and CPL. This inversion was accompanied by the morphological transition from nanofibers (*n*-BuOH) to fused spheres (PX/*n*-BuOH (1:1)) and nanoribbons (PX) (Figure 3f-g). This strategy developed by Liu et *al*, for constructing multicolor, chirality-switchable metal-organic supramolecular polymers has paved the way for the creation of photomodulated supramolecular polymers for writable information encryption applications, as demonstrated in a recent publication. These authors have also utilized the previously described **PTC**, **2**, exhibiting a *Z* configuration for the cyanostilbene moiety, that could be able to undergo *Z/E* isomerization and photocyclization upon exposure to ultraviolet or visible light giving rise to the corresponding complex with an *E* configuration for the cyanostilbene fragment (Figure 4).[16d] As stated before, ***Z*-2** is able to self-assemble into a supramolecular polymer in gel states using various organic solvents, which displayed negative CD and CPL signals at 469 nm, and 533 nm, respectively. Initially, these authors showed how **Z-PTC** also exhibited reversible CPL on/off switching and adjustable morphological changes between nanofibrous and fusiform structures upon altering exposure to 454 nm light irradiation and heating at 343 K. Interestingly, coordination of ***Z*-2** with silver ions in solvent mixtures, under ultrasonic treatment at room temperature, yields a supramolecular polymer (SP_1) with negative CD and CPL signal at 440 nm and 595 nm, respectively, which was distinct from those observed for the nanofibrous aggregate. In addition, a time-dependence of the ***Z*-2**/Ag^+ supramolecular polymerization was observed with the transformation of the deep yellow solution into yellow flocculent aggregates after 2h. This transformation suggests that the ***Z*-2**/Ag^+ supramolecular polymer can exist in both a metastable state denoted as metastable SP_{1m} and a thermodynamically stable state, referred to as stable SP_{1s} as was confirmed by time-dependent CPL measurements (Figure 4b). An initially negative CPL sign of metastable SP_{1m} at 595 nm gradually transformed into a positive CPL signal at 525 nm over a 30 min resting period (Figure 4b). Additionally, the formation of stable SP_{1s} was confirmed by a significant enhancement in the emission observed in the photoluminescence (PL) measurement, accompanied by a change in emission color from orange to yellow (Figure 4c). The results clearly demonstrate the dynamic assembly of ***Z*-2**/Ag^+, forming both metastable and stable supramolecular polymers. Moreover, *Z/E* isomerization of ***Z*-2**/Ag^+ assembly was studied under 454 nm light irradiation monitored by CD and CPL spectroscopy. Initial positive CD and CPL signals of SP_{1s}, at 469 and 545 nm, gradually shifted to negative signals, at 505 nm and 598 nm over a 30 min period upon exposure to the 454 nm light source, respectively (Figure 4d). These CD and CPL inversions indicate the formation of a new supramolecular polymer, SP_2 due to the Z to E

View Article Online
DOI: 10.1039/D5SC00729E

isomerization of ***Z*-2**/Ag^+ complex, in a reversible manner upon heating, as shown in Figure 4e.

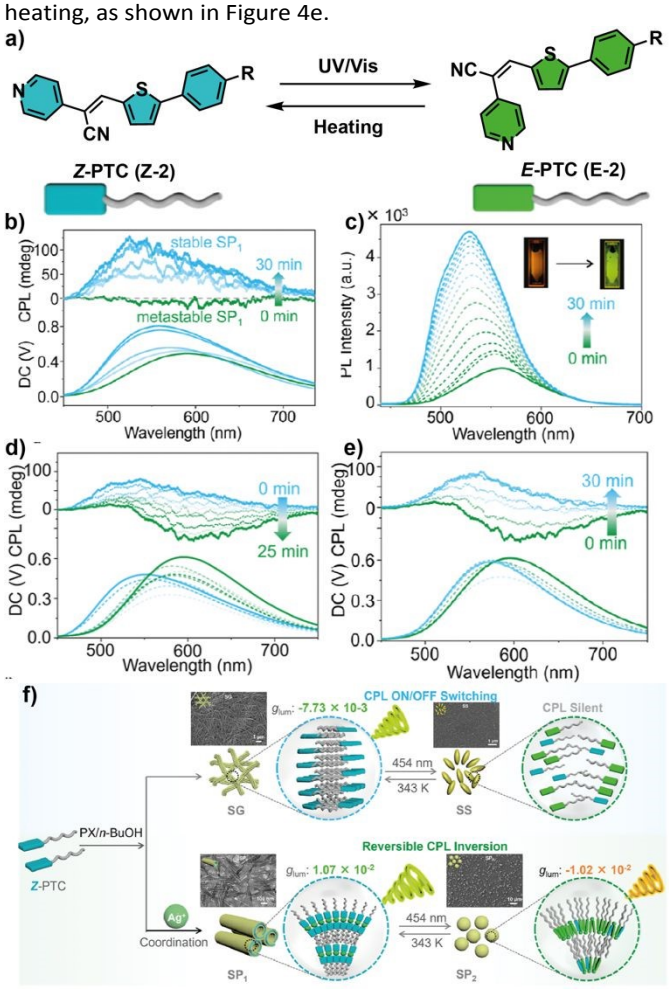

Fig. 4. (a) Reversible *Z/E* photoisomerization under 454 light irradiation and heating; (b) CPL and (c) PL spectra of ***Z*-2**/Ag^+ assemblies in PX/*n*-BuOH. The insets in Figure 4c show fluorescence photographs of ***Z*-2**/Ag^+; (d) and (e) CPL spectra evolution of SP_1 obtained from (d) under 454 nm light irradiation and (e) heated at 343 K for different times; f) Schematic illustrations of the CPL reversible transformation process of SG and SP_1 under 454 nm light irradiation and heating at 343K, respectively. Inset of SEM images of SG (up) and SP_1 (down) before and after irradiation (reprinted with permission from reference 16d. Copyright 2024 American Chemical Society).

The reversible chiroptical inversion was further evidenced by the associated structural transformation observed via SEM and transmission electron microscopy (TEM) measurements (Figure 4f). Initial observation showed nanotubes for SP_1, which transformed into nanospheres in SP_2 upon exposure to 454 nm light. Intriguingly, nanotubes reappear after 30 min incubation at 343 K. The result highlights the successful achievement of reversible chiroptical inversion, tunable emission characteristics, and morphological transition of SP_1 and SP_2 facilitated by 454 nm light irradiation and heating at 343 K (Figure 4f). Upon the introduction of Ag^+ ions, the resulting ***Z*-2**/Ag^+ complex assembles into laminar structures driven by π-π stacking interactions and hydrophobic effects. The laminar structures subsequently organize into nanotubes with hierarchical chirality transfer and amplification, accompanied by positive CPL emission at 545nm, with a g_{lum} value reaching up to 1.07 x 10^{-2}. Irradiating with 454 nm light involves a structural change from the linear structure of ***Z*-2**/Ag^+ to a more distorted structure in the ***E*-2**/Ag^+ complex. Consequently, the π-stacking interactions may be disrupted, leading the ***Z*-2**/***E*-2**/Ag^+ mixture complex to organize into nanosphere aggregates with inversion of CPL signal at 565 nm with a g_{lum} value of -1.02x10^{-2} (Figure 4f). Owing to their optical and chiroptical properties, these supramolecular polymers represent promising platforms for aggregated-state multimodal information encryption.

Following this approach, chloride-bridge-linked supramolecular polymers (**3**) can significantly enhance their chiroptical properties simply by decreasing the solvent polarity. In this case, the solvent acts as modulator provoking a intermolecular rotation motion in the dimer that cause a multiple chiroptical inversion (Figure 5a).[17] It was observed that, when using *p*-xylene as solvent rather than dichloromethane, a Zn(II) complex quickly forms, which subsequently aggregates into left-handed microhelices characterized by negative, cyan CPL emission (g_{lum}=-1.5x10^{-2}) (Figure 5b). However, over time, these micro-helices undergo a dynamic transformation into micro-belts with a clear reversal CPL emission and an increase in the g_{lum} value (g_{lum}=5.5x10^{-2}) (Figure 5b). Using techniques such as high-resolution electrospray ionization mass spectrometry (HR-ESI-MS), single crystal X-ray diffraction and theoretical calculations, they determined that *p*-xylene induces a molecular rotation in the **3** dimer that triggers the formation of distinct crystalline packing structures in addition to a dynamic chirality inversion. Furthermore, thermal treatment enhances the rotation of the coordinated complex dimer within the aggregates, leading to a secondary chiroptical inversion and the formation of well-ordered structures. Once equilibrium is reached a rapid transition in fluorescence from cyan to red was observed upon heating resulting in a structural transformation from micro-belts to well-ordered nanosheets as shown by SEM images (Figure 5c). Again, this conformational change is accompanied by an inversion of chirality and CPL signal (g_{lum}=-1.4x10^{-2}) (Figure 5b). These outcomes were also observed when xylene isomers, such as *o*-xylene and *m*-xylene, were used as solvent. In both cases, hydrogen bonding and CH-π interactions facilitate molecular rotation, giving rise to time-dependent CPL inversion. Upon thermal stimulation, cleavage of the chloride bridge is promoted, resulting in a secondary chiroptical inversion accompanied by a tunable shift in CPL emission color. This work provides a versatile platform for developing stimuli-responsive CPL-active systems with dynamically tunable chirality, offering potential for solid-state dynamic encryption applications, as will be discussed in the applications section.

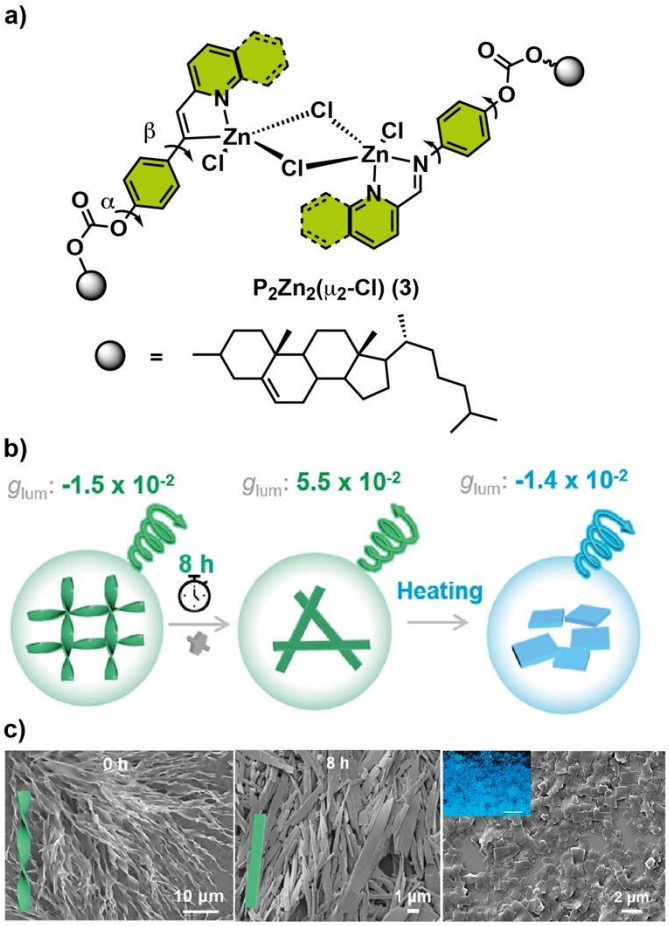

Fig. 5. (a) Chemical structure of the homochiral dimer molecular rotors linked by a chloride coordination bridge; (b) Schematic of the conformation transformation inducing dynamic multiple chirality inversion and tuneable CPL; (c) Time-dependent SEM microscopy images of ligand + $ZnCl_2$ aggregates in *p*-xylene at 0h, 8h and nanosheets obtained after heating the right-handed micro-ribbons of ligand +$ZnCl_2$ assembly. Inset: fluorescence microscope image of the nanosheets, with a scale bar of 10 mm (Reproduced from reference 17a with permission from Wiley-VCH, copyright 2025).

In contrast to aforementioned examples, in which metal coordination modulates the optoelectronic properties, an alternative approach would involve the deliberate incorporation of metal center into the molecular design to regulate intermolecular interactions, thereby governing the assembly process. Chen *et al.* create helical columnar emitters via thermally induced self-organization mediated by Pt-Pt contacts and π-stacking. They synthesized a pair of enantiomeric homoleptic Pt(II) metallomesogens (*R/S*-HPt) (**4a-b**) with pyridyltriazolate that features point chirality as cyclometalated ligands (Figure 6a).[18] This flexible side chain, in addition to increasing solubility and enantioselective assembly, promotes liquid-crystal behavior. UV-vis absorption and PL measurements reveal distinct spectra features in both solution and thin films. In dilute chloroform, two prominent high-energy absorption bands at 285 and 320 nm arise from the ligand-centered π-π* transition, while weaker low-energy bands at 368 and 383 nm are attributed to MLCT/ILCT processes, which is consistent with TDDFT analysis (Figure 6b-c). In spin-coated films, these transitions persist with slight bathochromic shifts (12-14 nm). Additionally, a broad new band near 450 nm emerges, assigned to MMLCT transitions, signifying strong intermolecular Pt-Pt and π-stacking interactions in the solid state. Polarizing optical microscopy (POM) measurements show that the enantiotropic hexagonal columnar mesophase is thermally stable. The materials form a highly stable Col_h^* mesophase (up to 358 °C), that shows high photoluminescence PL efficiency (ϕ up to 86%) and emits intense CPL at 615 nm (Figure 6b-c). When used in solution-processed chiral electroluminescent devices, they achieve high brightness, around 11379 cd·m^{-2}. However, the most remarkable is that the electroluminescence dissymmetry factor (g_{EL}) increases to 0.014, significantly better than many previously reported Pt(II)-based CP-EL systems.

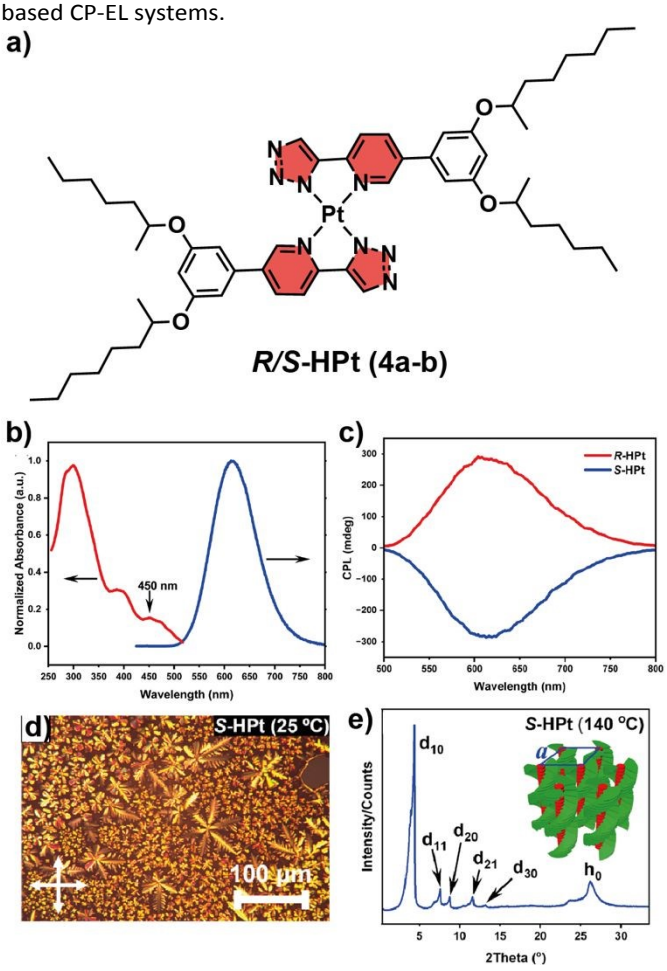

Fig. 6. (a) Chemical structure of the homoleptic Pt(II) complexes *R/S*-HPt **4a-b**; (b) Absorption and emission spectra of homoleptic Pt(II) complex T-HPt in spin-coated films; (c) CPL spectra after thermal annealing (d) POM images of *S*-HPt on cooling and (f) XRD profile of *S*-HPt (reproduced form ref. 18 CC BY).

As a final example in this section, we highlight the recent work by Tang *et al*., in which, in contrast to traditional strategies that rely on the use of opposite enantiomers to achieve inversion of

CPL signals, CPL inversion is regulated exclusively through control of the transition dipole moments, without altering the molecular or supramolecular chirality.[19] To that end, they developed new crystal materials based on axially chiral binaphthyl compounds that show solvent-induced CPL sign inversion. Two chiral Au complexes (*R/S*)-BPAuCz (***R/S*)-5**, based on binaphthyl and carbazole at terminal positions were synthesized (Figure 7). Remarkably, both enantiomeric Au-complexes exhibit different properties in solution and in the crystalline state. In THF solution, a weak PL was observed for both enantiomers with practically zero quantum yield, however, the addition of a polar solvent such as H_2O provoked a redshift in the emission wavelength of the Au coordination complex, attributed to enhanced intramolecular charge transfer, including ligand-to-ligand charge transfer (LLCT) and ligand-to-metal charge transfer (LMCT). This PL phenomena suggested that **(*R/S*)-5** were aggregate induce emission active (AIE-active). Besides, no CPL response was observed in THF solution of **(*R/S*)-5** even with aggregate solution in a polar solvent.

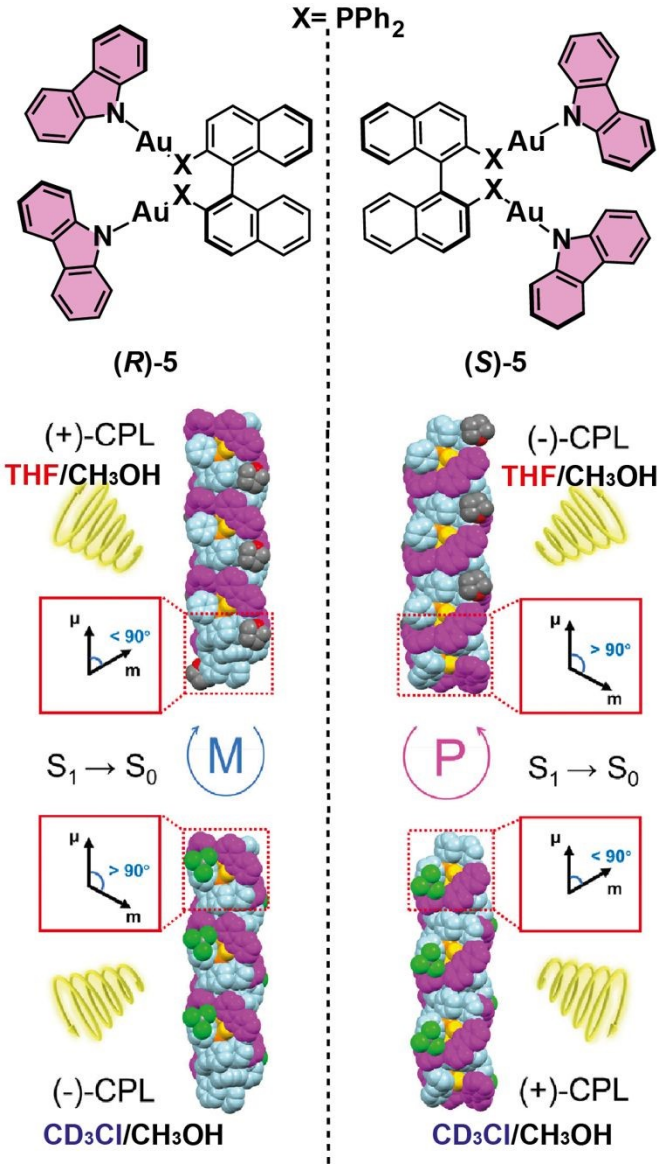

Fig. 7. Helical packing structures, circularly polarized luminescence signs, and transition dipole moment vectors of crystals **(*R/S*)-5** crystallized from solvents of THF/CH_3OH and $CDCl_3$/CH_3OH, respectively (reproduced form ref. 19 CC BY).

A different scenario was observed in the crystalline state. Using different techniques such as nuclear magnetic resonance NMR analysis, HRMS and single-crystal X-ray diffraction was evidenced that in both enantiomer crystal, the presence of two molecules of solvent in crystalline state, THF and $CDCl_3$, respectively. The single crystal for both enantiomers showed mirror-image symmetrical structures between *R/S*-stereochemical configurations with a dihedral angle of binaphthyls in the crystals of **(*R/S*)-5**^{T} and **(*R/S*)-5**^{C} of 90° because of the steric hindrance of carbazole Au(I) groups linked with 2,2´-binaphthyls. Single crystal of **(*R/S*)-5** obtained in THF and $CDCl_3$, exhibited photoluminescence quantum yields higher than those found in the aggregate solution, which were attributed to the tighter molecular packing in the crystalline states, thereby restricting the molecular motion. Because of the limited molecular motion, the molecules are strongly emissive in the crystal state. Moreover, CPL sign inversion with the same molecular chirality is observed in the crystalline state depending on the solvent used. **(*R/S*)-5**^{T} and **(*R/S*)-5**^{C} crystals exhibit left-handed CPL with g_{lum} of +9.81 x 10^{-4} and right-handed CPL with g_{lum} of -1.02x10^{-3} at 560 nm, respectively. These different CPL responses would be justified due to the influence of the weak interactions between different solvent molecules in the crystal structure, which may affect the transition dipole moments of the bulk crystal materials. To confirm this hypothesis, TD-DFT calculations revealed solvent-dependence with a different angle between magnetic and electric dipole moments (θ= 86.59° vs 95.89°), explaining the CPL inversion. Non-bonding interactions between solvent molecules and the AIEgens were found to control these optical properties. Additionally, the crystal demonstrated optical waveguide behaviour with loss coefficients of 187.3, 567.4, and 65.2 dB/cm for **(*R*)-5**^{T}, **(*R*)-5**^{C}, and **(*R*)-5**^{DCE}, respectively—showing potential for optical communication and integrated photonic devices.

This section offers an overview of recent developments in chiral coordination polymers displaying CPL activity. These advances contribute to a better understanding of the role of metals as key modulators of optoelectronic properties. Careful consideration of parameters such as metal geometry and valence is essential in the design of these systems, given their critical influence on molecular packing and chirality. In addition, external stimuli can regulate the dynamic behavior of these systems, thereby enhancing their functional properties. The following sections discuss the most significant advances in CPL-active supramolecular polymers, organized according to the origin of molecular chirality: point and axial chirality. Factors directly affecting the luminescence dissymmetry factor (g_{lum}) are highlighted, including the molecular design of π-conjugated monomers, the type of supramolecular polymerization mechanism, and the application of different external stimuli.

View Article Online
DOI: 10.1039/D6SC00729E

Point chirality in CPL-active supramolecular polymers.

In CPL-active supramolecular polymers, point chiral monomers serve as essential building blocks that dictate the macroscopic chiroptical properties of the system. Through cooperative self-assembly mechanisms in which hydrogen bonding, π-stacking, and metal coordination play a crucial role as non-covalent forces, local point chirality can induce long-range chiral order, leading to enhanced circular dichroism and circularly polarized emission. In this section, we focus our discussion mainly on some strategies where the application of common external physical stimuli, e.g. light and heat, or the chemical design can influence the structure organization and tuneable CPL properties of the supramolecular polymers.

One of the earliest examples using light to control the macroscopic helical sense of self-assembled structures was provided by Ajayaghosh and coworkers.[20] They demonstrate that the helicity of supramolecular assemblies defined by their inherent chirality can undergo a reversible switch to the opposite helical sense through chiral center mediated photoisomerization of the appended azobenzenes **6** and **7** (Figure 8). They synthesized azobenzene-linked phenyleneethynylene (PE) **6**-**7** derivatives to investigate light and heat controlled helical switching supramolecular assemblies. In THF, **(*S*)-7** exhibited monomer-like absorption bands at 324 nm and 419 nm. Upon switching to methylcyclohexane (MCH), these bands were red-shifted to 330 nm and 440 nm with an additional shoulder at 480 nm, consistent with aggregation. UV irradiation under MCH conditions provoked a *trans-cis* photoisomerization, forming mixtures of *E,Z* or *Z,Z* isomers (Figure 8a). This transformation was confirmed by the decrease in the absorption intensity at 330 nm, with a slight increase in the absorption intensity at 440 nm and the appearance of two isosbestic points (Figure 8b). A photostationary state (PSS) is attained within 15 minutes of irradiation with a 53% of conversion to the *cis*-isomers (*E,Z* and *Z,Z*) along with some remaining *E,E* isomers. It should be noted that the exact percentage of each isomer in the mixture could not be quantified due to the difficulty in separation by HPLC. Chiral derivatives **(*S*)-7** and **(*R*)-7** show strong, opposite CD and CPL signals before irradiation, indicating well-defined supramolecular helicity. Surprisingly, upon UV irradiation at 323 K and subsequent cooling, both compounds undergo a decrease in intensity and full reversal of their CD signals, demonstrating inversion of supramolecular handedness. The quantitative CD response from the chromophore excitonic coupling was estimated from the dissymmetry factor with values for $|g_{abs}|$= 0.0020 and 0.0022 for **(*S*)-7** and **(*R*)-7**, respectively (Figure 8b).

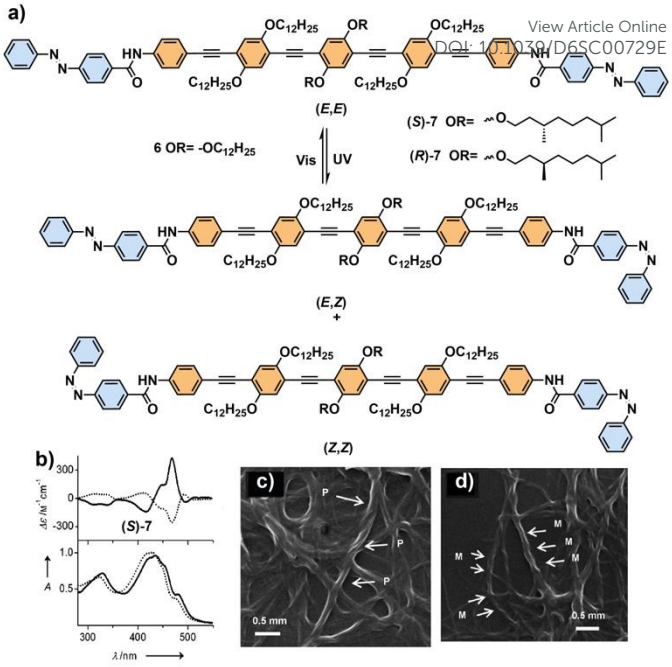

Fig. 8. (a) Photoisomerization of the azobenzene-linked phenyleneethynylene derivatives **6**-**7** (*R* or *S*). A mixture of *E,E*; *E,Z* and *Z,Z* isomers are possible; (b) CD spectra (top) and the corresponding UV absorption spectra (bottom) for **(*S*)-7** before (dash line) and after (dot line) UV irradiation; (c) SEM images of **(*S*)-7** before and (d) after photoisomerization. (Reprinted from reference 20 with permission from Wiley-VCH, copyright 2012).

Temperature-dependent CD studies reveal a change in the elongation temperature from 310 K to 303 K and a multistep assembly mechanism after isomerization, suggesting the coexistence of aggregates with different isomer compositions. They hypothesized that the initial nucleation may occur with the partially isomerized species present in higher concentration, with an inverted helicity, followed by the elongation of the helical chain with aggregates of the non-isomerized molecules with the initial *P*-helicity. Upon further cooling, aggregates of the fully isomerized molecules with lower stability and inverted helicity may also join the growing helices, further accelerating the overall opposite handedness. In addition, CPL measurements showed the same tendency after photoisomerization, the sign of CPL was reversed with a decrease in the g_{lum} value (g_{lum}=-0.002 at 503 nm) and (g_{lum} =+0.002 at 503 nm) for **(*S*)-7** and **(*R*)-7**, respectively. SEM and AFM imaging confirms that right-handed (*P*) helical ropes reverse to left-handed (*M*) helices after irradiation, as it is shown in Figures 8c-d. Helicity inversion requires heating above 313 K and proceeds through depolymerization followed by reassembly; without heating, irradiation alone does not change helicity. The process is reversible over multiple switching cycles. A mechanistic model was proposed that partially isomerized *E,Z* species dominate at the photostationary state and nucleate left-handed aggregates that direct subsequent supramolecular growth. Overall, the study shows that light and heat can reversibly switch the macroscopic helicity of supramolecular

View Article Online
DOI: 10.1039/D6SC00729E

assemblies without altering molecular chirality. This principle was useful for designing responsive materials with switchable optical or electronic properties.

Another pioneer example, described by Kumar et al, demonstrated that bichromophoric systems not only can function as scaffolds to enhance chirality amplification in supramolecular assemblies but also display high CPL emission.[21] They synthesized two *trans*-1,2-diamide-ciclohexane derivatives covalently linked to two chromophoric units of PDIs which differ in the nature of the spacer between them (Figure 9a). Whilst compound **8** is endowed with a glycine unit as spacer, in compound **9** β-alanine acts as the spacer. This subtle increase in the spacer length between the PDI and the cyclohexane moiety helped in reversing the direction of the chiral arrangement of PDI units connected to the identical chiral center and also controlling the degree of overlap between the PDI units. Initial UV-vis and fluorescence spectroscopic studies of both molecules in a good solvent as chloroform indicate that the molecule remains in the monomeric state, however, slight but discernible changes were observed such as the decrease in the relative absorbance of $A_{0\text{-}0}/A_{0\text{-}1}$ a more prominent shoulder above 630 nm in emission, characteristic to the excimer-like state and longer emission decay for the excimer state for **9** relative to **8**. These differences suggested a stronger overlap of the PDI units in **9** that also was observed through CD spectra with an additional strong CD band at 550 nm. Additionally, the chiral nature in fluorescence was characterized by using CPL spectra. The luminescence dissymmetry factor in both compounds at 540 nm matches well with the quantitative CD response from the exciton coupling (g_{lum}=6 x10^{-4}, g_{CD}=4x10^{-4}) and is among the typical values reported for such bichromophoric systems in the solution phase. However, in compound **9**, an additional peak with opposite sign and a large g_{lum} value of 8x10^{-3} was observed at 630 nm. This band might be attributed to the decay from the excimer-like state as suggested by lifetime measurement, which could correspond to the inter-PDI excitation. The CPL sign in the monomeric state correlates with the CD band at the longest wavelength, confirming an intermolecular electronic transition between PDI units governed by their relative P/M configuration. In contrast, excimer CPL exhibits an opposite sign due to a transition dipole oriented perpendicular to the exciton-coupled state. Therefore, the flexibility of compound **9** enhances CD and CPL responses by increasing PDI-PDI overlap (Figure 9c-d).

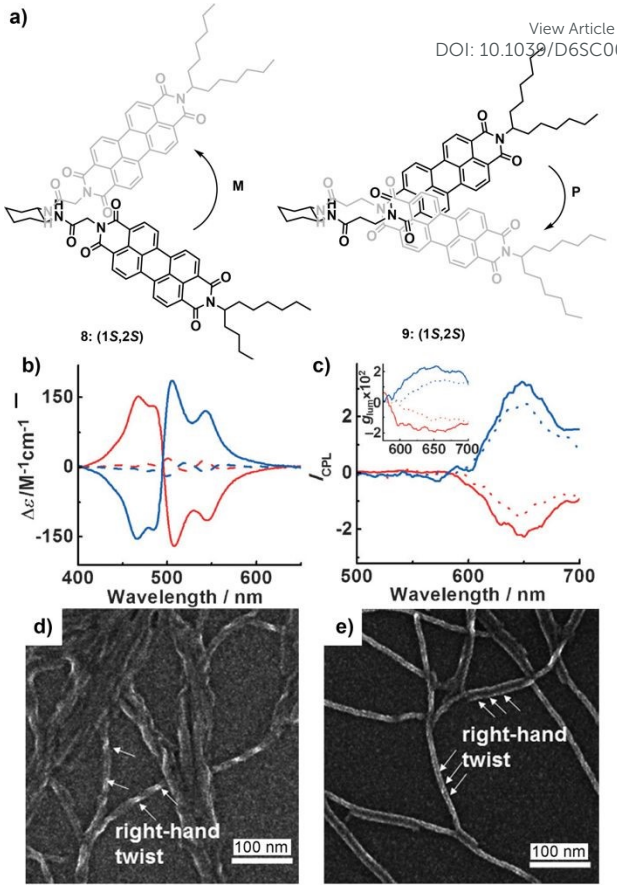

Fig. 9. (a) Molecular structures of compounds **8** (1*S*,2*S*) and **9** (1*S*,2*S*) and schematic representation of the chiroptical properties in the monomeric and assembled states; (b) CD spectra of the *R* (red lines) and *S* (blue lines) isomers of **8** (broken lines) and **9** (solid lines) in MCH; (c) CPL spectra of the *R* (red lines) and *S* (blue lines) isomers of **9** in MCH (solid lines) and chloroform/MCH mixture (dotted lines). The inset in (c) shows the corresponding g_{lum} spectra of **9**; (d) SEM images of (1*S*,2*S*)-**9** and their magnified images (e) (Reprinted from reference 21 with permission from Wiley-VCH, copyright 2013).

The aggregation behaviour of these PDI-based compounds was studied in $CHCl_3$/MCH mixtures as solvent. Increasing the MCH content resulted in a redshift of the absorption peak and significant quenching of the monomeric PDI fluorescence emission. This was accompanied by the emergence of a new, intense emission band at longer wavelength. These outcomes revealed the transition from the monomeric state to aggregates through intermolecular hydrogen bonding and auxiliary π-stacking between the PDI units. Slight differences were also observed in the supramolecular aggregates, with better PDI organization in the self-assembled structures of **9** versus **8**, leading to more efficient energy migration, higher emission quantum yield and longer emission lifetime. These aggregates tend to form helical fibres, being more tangled and denser for **8** and more flexible, long and thin for **9** (Figure 9d-e). It is worth noting that identical helicity was observed in both cases, regardless of the opposite arrangements of perylene moieties in the monomer unit. This fact clearly suggests that the central

View Article Online
DOI: 10.1039/D5SC00729F

cyclohexane-diamide unit is responsible for the supramolecular helicity of the self-assembled structures, which was also confirmed by CD spectra. Interesting outcomes were observed in CPL for **9** showing g_{lum} values nearly an order of magnitude higher than the monomer (g_{lum}= 0.025) as well as a sign inversion. This value was among the highest reported for organic chromophores in solution at that time. Solid-state CPL studies of the aggregates revealed that **9** formed helical networks of fibrous assemblies, exhibiting an intense CPL signal with a g_{lum} value of 0.035, slightly higher than that observed in solution. This bichromophoric systems were one of the first examples where tuneable chiroptical properties were achieved with large g_{lum} values in solution and solid state.

Our research group published another example in which a bias in the CPL response occurs, directly dependent on the nature of the central π-conjugated unit as well as on the aggregation process.[22] In this case, two pairs of enantiomeric cyano-luminogens (**10** and **11**) based on *p*-phenylene or a 2,5-dithienylbenzene moiety as central chromophore functionalized with four benzamide units, promote supramolecular polymerization through quadruple hydrogen-bonding arrays between the amides and the π-stacking of the central aromatic core (Figure 10). The presence of chiral alkyl side chains induces helicity in the resulting assemblies, making them suitable platforms to explore both kinetically and thermodynamically controlled supramolecular polymerization and the influence on chiroptical and emissive properties. The peripheral benzamide groups can form intramolecular hydrogen-bonded pseudocycles, giving rise to metastable monomers (*M**). These monomers generate kinetically controlled aggregates (AggI), which can evolve into thermodynamically more stable aggregates (AggII). The self-assembly process was studied by UV-vis and CD spectroscopy and AFM imaging, revealing distinct aggregation pathways for compounds **10** and **11** (Figure 10a-e). For compound **10**, AFM confirmed the evolution from thin helical filaments (AggI) into thicker superhelical fibers (AggII). In contrast, compound **11** initially forms nanoparticles (AggI) that reorganize into fibrillar helical structures (AggII), highlighting differences in aggregation driven by the central aromatic unit. CD studies demonstrated that the supramolecular aggregates of both systems are chiroptically active, but their responses depend on the aggregation pathway. Compound **10** showed a bisignated CD response of the same sign for both AggI and AggII, consistent with the formation of helical aggregates. Compound **11**, however, exhibited a stereomutation phenomenon: during the transition from AggI to AggII, the CD signal inverted its sign, indicating a change in helicity. This stereomutation underscores the sensitivity of supramolecular chirality to kinetic versus thermodynamic assembly. The emission properties were also found to be aggregation-dependent.

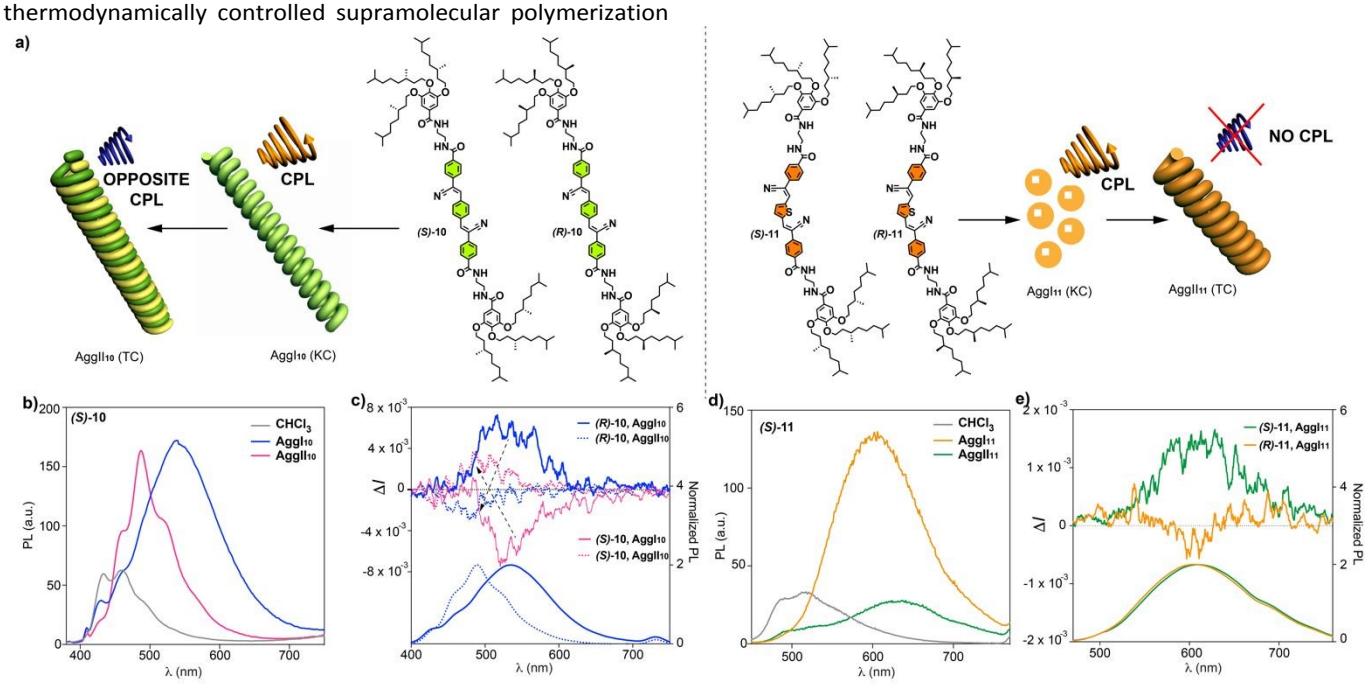

Fig. 10. (a) Chemical structures of chiral cyano-luminogens (central part) and schematic representation of the CPL-emitting kinetic and thermodynamically controlled aggregated structures formed by **10** and **11**; PL (b and d) and CPL ((c) and (e)) of (*S*)-**10** ((b) and (c)) and (*S*)-**11** ((d) and (e)) spectra in monomeric and aggregated states ($CHCl_3$ and 9/1 MCH/$CHCl_3$ mixture, respectively. Dashed arrows in panel (c) indicate the inversion of the CPL sign (reproduced form ref. 20, CC BY).

For compound **10**, both AggI and AggII displayed strong photoluminescence due to the AIE effect and significant CPL activity, but with opposite CPL signs between the two aggregate states as shown in Figure 10b-c. The value of the dissymmetry factor for these kinetically controlled AggI species was ~ 0.007 (λ_{exc}= 365nm) and aging the solution of AggI for 24 h to ensure the complete conversion to AggII resulted in a sign inversion with a slightly g_{lum} decrease value (~ 0.004) (Figure 10b-c). For compound **11**, AggI exhibited strong AIE and detectable CPL, but upon conversion to AggII, the system underwent aggregation-caused quenching (ACQ), and CPL activity was lost (Figure 10d-

View Article Online DOI: 10.1039/D5SC00720F

e). These contrasting behaviours demonstrate how subtle changes in molecular design (phenylene vs. thienyl core) lead to markedly different emissive and chiroptical outcomes. This work highlights how supramolecular polymerization pathways critically influence morphology, chirality, and optical properties in chiral cyano-luminogens. While phenylene derivatives **10** maintain CPL activity with sign inversion between AggI and AggII, thienyl derivatives **11** undergo stereomutation and CPL cancellation upon thermodynamic reorganization. These findings expand the understanding of dynamic supramolecular chirality and show how controlled self-assembly can be harnessed to modulate CPL activity, emission behaviour, and aggregate morphology, with implications for applications in chiroptical devices, sensing and optoelectronics.

Inspired by nature systems, where the formation of highly organized helical structures results from multiple interactions governed by cooperative growth, Wang *et al.* designed another more extended π-conjugated system based on a dicyanostilbene core for the development of CPL detection materials.[23] Two chiral dicyanostilbene derivatives, **(*S*)-12** and **(*S*)-13** were synthesized, with dual amide functionalities flanking the π-core to promote π–stacking and hydrogen bonding through a cooperative growth (Figure 11a). The (*1S*)-phenylethyl groups imparted point chirality to bias supramolecular helicity. An achiral analogue, compound **14**, was also designed for chirality amplification studies by co-assembly with a small fraction of the enantiopure compounds. UV–Vis, fluorescence, and temperature-dependent spectroscopic analyses confirmed cooperative supramolecular polymerization in nonpolar solvent (methylcyclohexane) for (*S*)-**12** as shown in Figure 11. In UV-vis, a blue shift was observed for the π-π* absorbance band, accompanied by the emergence of a shoulder band between 442 and 500 nm whilst a red shift from 488 nm to 570 nm was detected for the maximum fluorescence emission signal (Figure 11b). AFM images revealed the formation of micrometer-long nanofibers, consistent with one-dimensional polymeric growth (Figure 11d). Supramolecular chirality emerged upon one-dimensional polymerization of **(S)-12** in MCH.

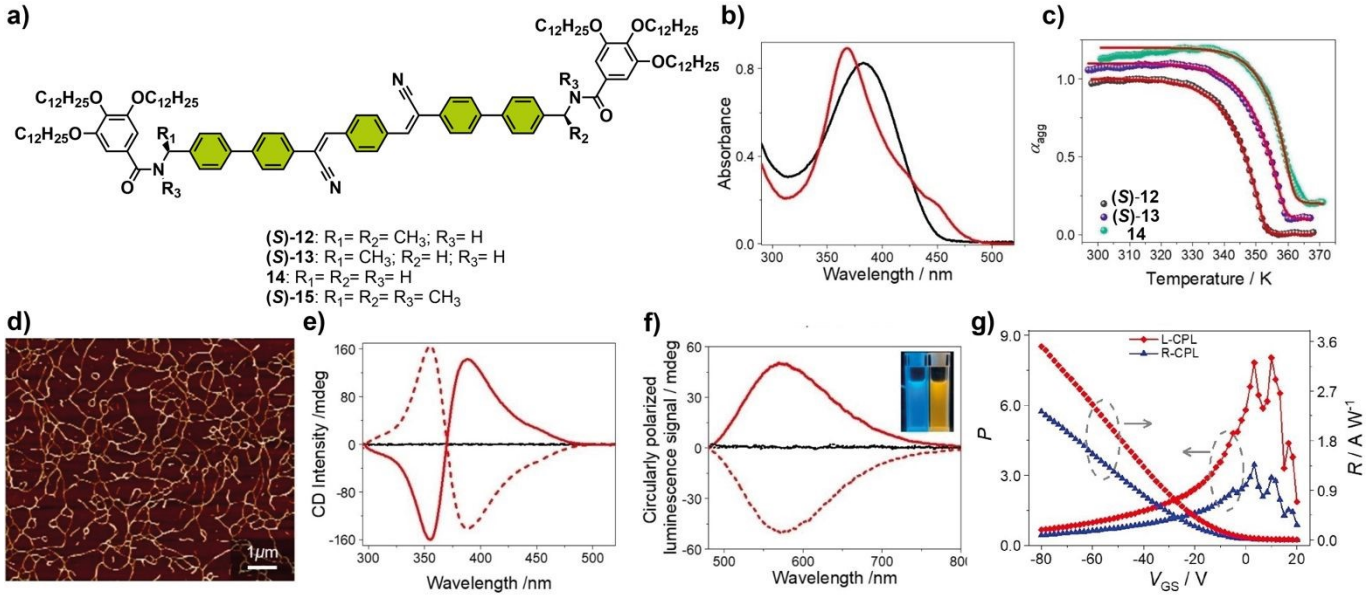

Fig. 11. (a) Chemical structures of the chiral monomers **(*S*)-12** or **(*S*)-13**, the achiral monomer **14** and the control compound **(*S*)-15**; (b) UV/Vis spectra of **(*S*)-12** in $CHCl_3$ (black line) and MCH (red line); (c) α_{agg} as a function of temperature for compounds **(*S*)-12**, **(*S*)-13**, and **14**, by monitoring the absorbance intensity changes at 388 nm (d) CD and (e) circularly polarized luminescence spectra of **(*S*)-12** (solid red lines and **(*R*)-12** (dash red lines) in MCH. The spectra of the two compounds in $CHCl_3$ are shown in black. Inset of (e): photographs of **(S)-12** in $CHCl_3$ (left) and MCH (right) under a 365 nm ultraviolet lamp; (f) AFM height image of **(*S*)-12**; (g) The photosensitivity P, and photoresponsitivity R values of OFETs based on the **(*S*)-12** supramolecular polymers upon exposure to 450 nm LCP or RCP irradiation (reprinted from reference 23 with permission from Wiley-VCH, copyright 2023).

In the π-π* absorption region, a bisignated Cotton signal was detected, consisting of a positive band at 388 nm (anisotropy factor g_{abs} value= 0.00716) and a negative band at 354 nm (g_{abs} =-0.00707). Concurrently, a positive CPL response was observed at 573 nm, yielding a g_{lum} value of 8.3 x 10^{-3} (Figure 11e-f). In addition, density functional theory (DFT) and FTIR analyses for **(*S*)-12** verified dual noncovalent interactions (π–stacking and H-bonding) as key drivers of the cooperative assembly. In contrast to derivative **15**, in which the amides were methylated, neither supramolecular chirality nor fibrous morphology was detected, despite evidence of π-stacking interactions. Notably, these systems were used to fabricate organic field effect transistors (OFETs), using the poly(3-hexylthiophene-2,5-diyl) (P3HT) as π-type semiconductor. The devices displayed excellent charge carrier transport capability with values of a threshold voltage (V_{th}), maximum field-effect electron mobility (μ), and on/off ratio (I_{on}/I_{off}) of the device from **(*S*)-12** of -19.8 V, 0.0044 $cm^2V^{-1}s^{-1}$, and 8.5 x 10^4, respectively. Remarkably, OFETs based on **(*S*)-12** demonstrated a selective photoresponse with a clear discrimination between left- and right-CPL, yielding a

pronounced increase in current and substantial shift in threshold voltage from -19.8 V to -7.8 V under L-CPL illumination. Moreover, the responsivity parameter g_R value of OFETs from **(*S*)-12** and **(*R*)-12** were quantified to +0.83 and -0.82, respectively, being one of the highest values observed for π-conjugated supramolecular assemblies. The principal distinction between these systems lies in the supramolecular polymerization mechanism, which follows a nucleation-elongation pathway rather than an isodesmic process.[24] Cooperative polymerization appears to promote a higher amplified dissymmetry factor for circularly polarized photodetectors, diving in part by enhanced exciton coupling between adjacent dicyanostilbene units and the size compatibility between the self-assembled polymers and the wavelength of the CPL, resulting in g_R values for the OFETS that exceed the g_{abs} values of compound **(*S*)-12** in film.

Other weaker interactions, such as CH-π, also contribute to the generation of supramolecular systems exhibiting CPL activity. Chiral systems based on styrylpyrene (**(*S*)-16a** and **(*R*)-16b**) utilize this weak interaction to self-assemble into helical nanoribbons via cooperative polymerization, preserving their emission properties (Figure 12).[25] UV-vis and circular dichroism studies revealed that **(*S*)-16a** undergoes cooperative supramolecular polymerization in a mixture solvent such as methylcyclohexane:tetrachloroethane (MCH/TCE, 24:1 v/v). In this condition, a blue shift of the maximum absorption band appears, accompanied by new shoulders at 328 nm and 432 nm, as well as a bisignated Cotton effect with positive and negative signals at 392 nm and 356 nm (Figure 12b). These features indicate π-π offset stacking and the formation of right-handed helicity. In contract to the results in mixed solvents, pure TCE yielded no detectable CD signal. These outcomes unveiled that chirality transfer arises from supramolecular organization. However, variable concentration NMR and fluorescence measurements of **(*S*)-16a** showed no change in the chemical shift of either the amide or aromatic protons, ruling out hydrogen bonding and π-stacking as dominant interactions in the resulting aggregates. Moreover, the emission profiles of **(*S*)-16a** in both its monomeric and aggregated form remained nearly identical, indicating weak electronic coupling between pyrenes units. Finally, 2D NOESY spectra confirmed that the aggregates formed arise edge-to-face CH-π contacts, evidenced by cross-peaks between phenyl C-H and pyrene protons.

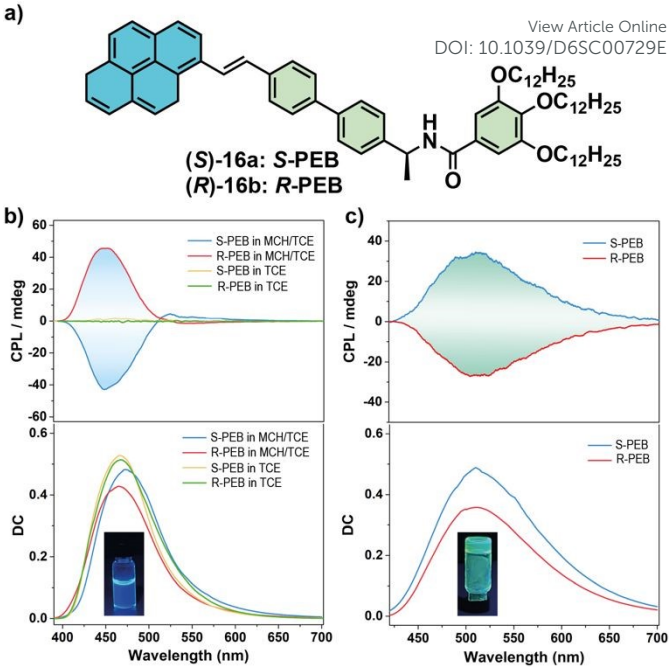

Fig. 12. (a) Structure of monomers *S*-PEB (**(*S*)-16a**) and *R*-PEB (**(*R*)-16b**); (b) CPL and fluorescence spectra (up and down) of (**(*S*)-16a** and **(*R*)-16b** in MCH/TCE and TCE solution. Inset: the fluorescence image of **(*S*)-16a** in MCH/TCE solution; (c) CPL and fluorescence spectra (up and down) of **(*S*)-16a** and **(*R*)-16b** gel samples formed in MCH solution. Inset: the fluorescence image of **(*S*)-16a** gel (reported from ref 25, CC BY).

Complementary DFT analyses showed that CH-π interactions dominate the antiparallel twisted stacking mode of **(*S*)-16a** dimers, leading to stable helical supramolecular polymers. This is an exceptional case where CH-π contacts, rather than π-π stacking or hydrogen bonding, dictate supramolecular helicity. Furthermore, different fluorescence behaviour and a handedness-inverted CPL signal were observed for both enantiomers in solution and gel state. In solution, aggregated *S*-PEB displayed bright blue fluorescence λ_{em}=461 nm with high Φ_F=69% and a negative CPL signal at 441 nm with a g_{lum} value of -0.001 (Figure 12b). While in the gel state, yellow-green emission (λ_{em}=498-526 nm and Φ_F=39%) was observed due to the stronger packing besides a positive CPL signal at 510-520 nm g_{lum}=+0.0053) (Figure 12c). This colour-dependent handedness inversion occurs without inversion of supramolecular chirality, as confirmed by identical CD spectra for both cases.

Theoretical CPL simulations corroborate that stacking geometry affects the CPL sign, explaining the opposite handedness between the blue (solution) and yellow-green (gel) states. Such behaviour-dual CPL handedness without chirality inversion is exceptionally rare in single component systems. Moreover, drop-cast and PMMA-embedded films were prepared and showed strong yellow-green CPL with g_{lum}=+0.001 and Φ_F=26%, consistent with the gel state. The CPL sign is preserved across the gel, film and PMMA composite forms, demonstrating structural stability and reproducibility. This work established a versatile strategy for multi-modal, colour-switchable CPL materials using a single chiral chromophore. Furthermore,

present an additional advancement, the study of the photoreactive behaviour of helical supramolecular polymers derived from stilbene-pyrene. Supramolecular confinement provides spatial proximity of the classical photoactive double-bond moieties. This allows the photoinduced [2+2] cycloaddition reaction in the supramolecular **(*S*)-16a** solution being faster than in the monomeric solution. This finding opens new avenues for obtaining photoresponsive chiral optoelectronic devices from light-controlled supramolecular systems.

In the design of π-conjugated systems exhibiting CPL activity, it is important to consider the restriction of intramolecular motions. In any cases, this restriction of intramolecular rotation can promote a staggered arrangement of the monomer, leading to the formation of *J*-type supramolecular polymers with an enhance in the emission dissymmetry factor and quantum yield, as seen in the chiral anthraquinone-based compounds, **(*S*)-17a** and **(*S*)-18** (Figure 13a).[26] In both compounds, amide groups promote supramolecular polymerization through hydrogen bonding and π-stacking interactions. However, in **(*S*)-17a**, the inclusion of the acetylene spacer enforces an almost coplanar geometry between the anthraquinone and phenyl units with a torsion angle of 1.81°, favoring efficient slipped *J*-aggregation. This optimized packing facilitates effective chirality transfer from sterocenters to the emissive core as well as induces a significant change in the emission pathway from cyan fluorescence in the monomeric state to yellow phosphorescence in the polymeric form, with emission lifetime increasing 71-fold. Quantum yields improved sevenfold, and g_{lum} reached 0.031 with a high CPL brightness value of 13.8 $M^{-1}cm^{-1}$, that exceeds the typical detection threshold for point-chiral organic luminophores (Figure 13b-c). This improvement is also evident in the formation of long-range-ordered 1D nanofibers with length of a few micrometers and an average height of 4.7 nm, as observed by AFM. Conversely, **(*S*)-18**, which lacks acetylene linkers, exhibits a significantly twisted conformation with an angle about 33.4°. This distortion disrupts *J*-aggregation, leading to complete quenching of CPL activity with the formation of nanoparticles as it was observed in AFM images. Additionally, Förster resonance energy transfer (FRET) was integrated by doping **(*S*)-17a** assemblies with the red-emissive acceptor **19**. This enables color-tunable CPL, shifting emission from yellow to red while significantly boosting efficiency (quantum yield up to 41.7%) and dissymmetry (g_{lum} = 0.060). Prototype CPL-emitting LED devices exhibited strong, stable CPL signals with excellent reversibility under electrical driving, confirming their potential for practical chiral optoelectronic applications.

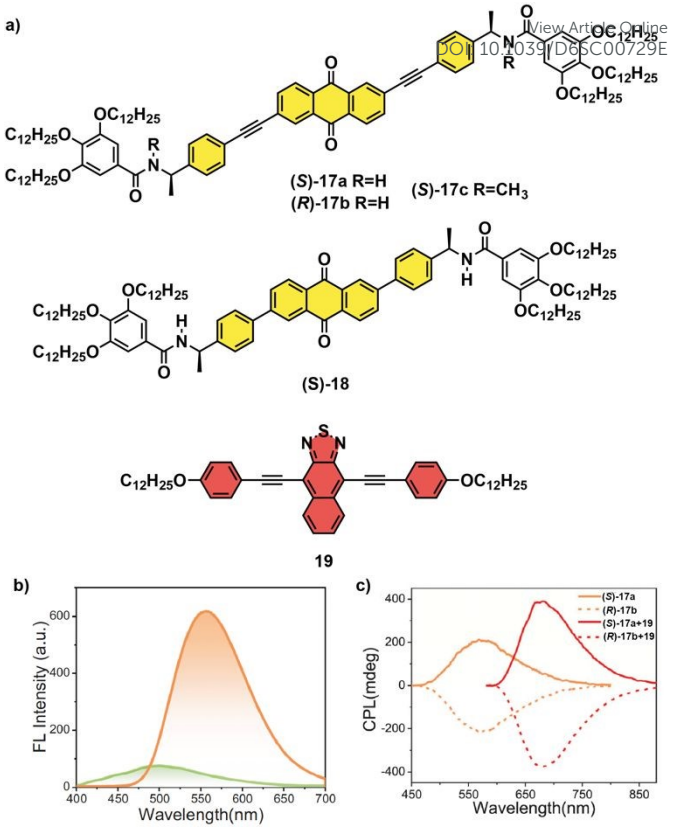

Fig. 13. (a) The chemical structures of compound **(*S*)-17a-b**, control compound **(*S*)-17c** and **18**, and energy acceptor **19**; (b) Emission spectra of **(*S*)-17a** in chloroform (green line) and methylcyclohexane (orange line) upon excitation at 365 nm; (c) CPL spectra of the supramolecular polymeric films of **(*S*)-17a**, **(*R*)-17b** and binary complex **(*S*)-17a** + **19** or **(*R*)-17b** + **19** upon excitation at 365nm. (Reproduced from reference 26 with permission from Wiley- Wiley-VCH, copyright 2025)

Additionally, another interesting strategy reported by Wang *et al.* involved the incorporation of intermolecular charge-transfer complexation into chiral supramolecular polymers to achieve tuneable CPL.[27] Specifically, two enantiopure triphenylamine donors **(*R*)-20** and **(*R*)-21** were synthesized. In one case, *N*-[(1*R*)-phenylethyl]benzamide units are incorporated at the peripheries of the triphenylamine core in **(*R*)-20**, while in **(*R*)-21** these substituents lack the acetylene linkages, as illustrated in Figure 14a. Both donors **(*R*)-20** and **(*R*)-21** self-assemble into helical supramolecular polymers through threefold hydrogen bonding via cooperative nucleation-elongation mechanism as confirmed by the temperature-dependent experiments. The only experimental difference between two supramolecular polymers was that **(*R*)-21** showed higher thermo-stability and stronger gelation tendency than **(*R*)-20** under identical conditions. These phenomena were attributed to different twisting of the triphenylamine cores. The lack of acetylene linkages provokes an increase in the rotation angles from 6.5° in the trimeric species **(*R*)-20**$_3$ to 11.9° in **(*R*)-21**$_3$, resulting in strengthened hydrogen bonding with intermolecular N-H•••O distances between adjacent amides: 1.85-18.9A in **(*R*)-20**$_3$ versus 1.82-1.86 A in **(*R*)-21**$_3$, which was confirmed by DFT

View Article Online
DOI: 10.1039/D5SC00790E

calculations. This finding aligns with the Gibbs free energy changes observed in the supramolecular polymerization process, indicating that **(*R*)-21** is 2.3 KJ/mol higher in energy compared to **(*R*)-20**. Moreover, supramolecular homopolymers of **(*R*)-20** and **(*R*)-21** displayed blue-coloured CPL with g_{lum} value at 472 and 453 nm of -7.2x10^{-3} and 9.4x10^{-3}, respectively (Figure 14b-c).

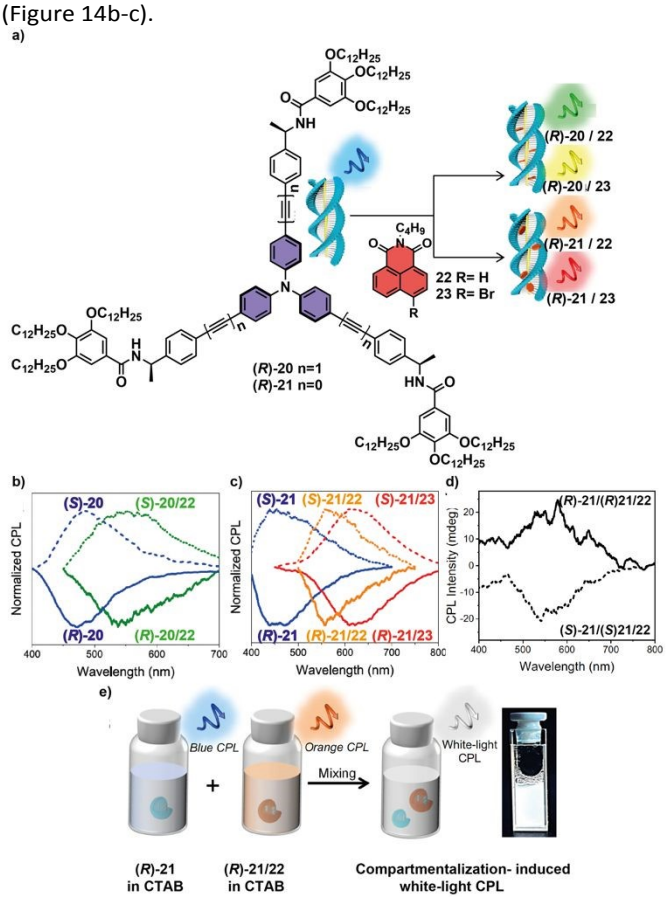

Fig. 14. (a) The chemical structures of the triphenylamine donor compounds **(*R*)-20** or **(*R*)-21**, the naphthalenemonoimide acceptor compound **22** or **23** and schematic illustration for wide-range tuneable circularly polarized luminescence of supramolecular donor-acceptor polymers via intermolecular charge-transfer complexation; (b and c) Normalized CPL spectra of supramolecular donor polymers **20** and supramolecular donor-acceptor polymers **20/22** in the film state (b) and **21**, together with supramolecular donor-acceptor polymers **21/22** and **21/23** in the film state upon excitation at 365 nm (c); (d) Mirror-imaged CPL of white-light emissive **(*R*)-21/22** and **(*R*)-21/23** (solid line) and **(*S*)-21/22** and **(*S*)-21/23** (dotted line) aqueous solutions encapsulated in CTAB; (e) Schematic illustration of preparing white-light luminescence of **(*R*)-21/22** encapsulated in CTAB. (Reproduced form ref. 27, CC BY-NC-ND).

At this point, the introduction of naphthalenemonoimide (NMI) acceptors (**22** and **23**) into the homopolymers allows the formation of the donor-acceptor complex. Here, the modulation of the CT strength is achieved through adjustments to structural features such as acetylene linkages on triphenylamides donor, which modify the HOMO energy levels or bromination on NMI, which alter the LUMO energy levels, providing supramolecular donor-acceptor polymers with tuneable CPL signals. These CPL signals vary from green and yellow, obtained for supramolecular donor-acceptor polymers **(*R*)-20/22** and **(*R*)-20/23**, to orange and red colours for **(*R*)-21/22** and **(*R*)-21/23**, respectively (Figure 14b-c). These subtle structural variations dictate the donor-acceptor packing modes, which, in turn, control ground-state versus excited-state CT pathways, resulting in distinct emission wavelengths and lifetimes. The study further resolves challenges in achieving white-light CPL by employing surfactant-based micellar compartmentalization, allowing blue-emitting TPA polymers and orange-emitting CT complexes to coexist without mutual quenching (Figure 14d-e). Overall, the work demonstrates that precise manipulation of CT interactions within chiral supramolecular polymers provides a robust and modular approach for designing CPL-active materials with full-spectrum tunability, suitable for advanced photonic and display technologies.

Giuseppone, Bassani and Moulin propose the first supramolecular polymer in which the handedness of the emitted circularly polarized light can be switched-using the same enantiopure building block merely by adjusting the cooling speed during self-assembly.[28] This effect has been attained by the self-assembly of the two chiral triarylamine-based monomers **TATA-24** and **TATA-25** (Figure 15). In the first one, *C*$_3$-symmetric **TATA-24**, three tetraphenylethene (TPE) fluorophores units are connected to the TATA core through three linkers containing (*S*) sterocenters based on citronellol. In the second monomer, **TATA-25**, a single TPE unit is linked to the TATA core through an achiral chain, while the chirality of the self-assembly is directed by two additional chiral side arms. They first examined the self-assembly behaviour of both monomers by controlling the cooling of their chlorobenzene solutions using two different protocols; fast cooling, in which a hot solution is cooled directly to -20 ˚C and slow cooling, where the temperature is decreased at a controlled rate of 0.5 ˚C/min or slower. Using AFM and TEM imaging, these authors observed that monomer **TATA-24** formed thick, bundled fibrillar aggregates under rapid cooling. These structures consisted of irregular fibers of 7-10 nm diameter, intertwined into *M*-type superhelical domains (Figure 15b). In contrast, slow-cooling produced straight, more ordered flat ribbons with widths from 10-50 nm and a uniform height of 2 nm, composed of parallel fibrils spaced about 3 nm (Figure 15b).

View Article Online
DOI: 10.1039/D6SC00729E

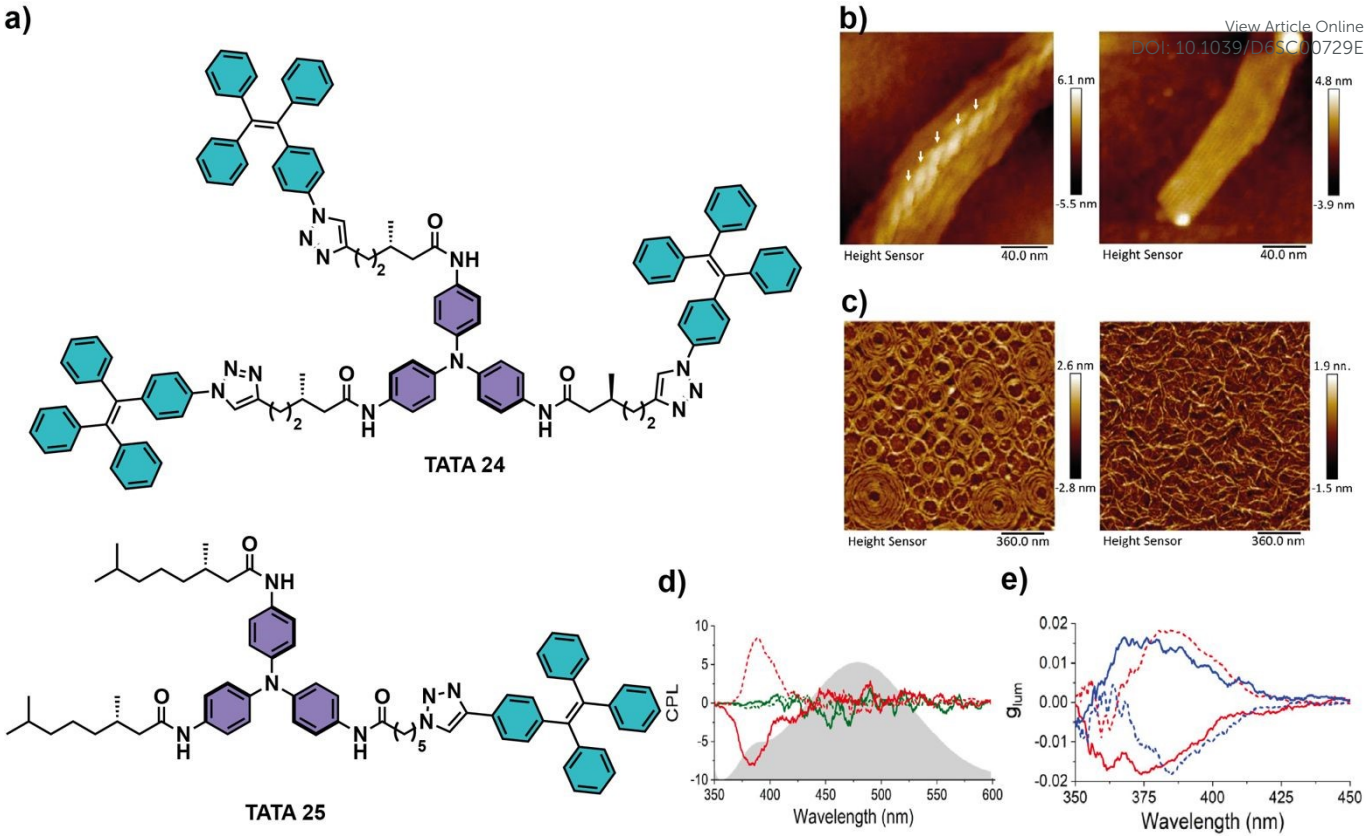

Fig. 15. (a) Structure of monomers **TATA-24** and **TATA-25**; (b) AFM micrographs of the self-assembled structures obtained of **TATA-24** fast cooling (left); slow cooling (right); (c) **TATA-25**, fast cooling (left), slow cooling (right); (d) CPL spectra of **TATA-24** (green) and **TATA-25** (red) obtained by fast cooling (dashed line) and slow cooling (solid line) and emission spectra of **TATA-25** obtained by slow cooling (grey area); (e) g_{lum} values of **TATA-25** red for the *S* enantiomer, blue for *R* enantiomer obtained by fast cooling (dashed line) and slow cooling (solid lines) (Reproduced form ref. 28, CC BY-NC-ND).

On the other hand, monomer **TATA-25** upon fast-cooling produced flat, circular objects with heights of 2 nm, composed of loosely aggregated single fibrils exhibiting *P*-type helicity. When the sample was slowly cooled, it instead formed twisted fibers that further intertwined into larger, diffuse microgel networks (Figure 15c). These fibers display twisted segments characteristic of *M*-type superhelical arrangements, generated by the coiling of 2-3 single fibrils. These distinct structures arise from competition between primary nucleation growth under fast cooling and secondary nucleation/elongation growth under slow cooling. In addition, chiroptical and spectroscopic properties were studied for both monomers and also showed differences between the two cooling regimes. The absorption spectra exhibited a blue shift in the aggregate state of **TATA-24** and **TATA-25** monomers compared with dissolved state monomers, confirming the formation of *H*-type aggregates. The slow-cooled samples gave weaker absorption intensities than the fast-cooled ones, indicating stronger electronic interaction between the TATA units in former self-assemble structures. CD experiments revealed bisignated CD signals, with opposite signs under fast and slow cooling, which matched with the helicities observed via AFM. It is noteworthy that the CD intensities for **TATA-25** were stronger than **TATA-24**, suggesting better chromophore organization. This tendency was also observed in the emission spectra. **TATA-24** and **TATA-25** displayed AIE due to the presence of TPE, however, **TATA-25** emitted more intensely despite having fewer TPE units, showing that supramolecular packing dominates emission behaviour. Finally, the ability of self-assemblies to emit circularly polarised light was investigated. While no CPL signal was observed for **TATA-24**, **TATA-25** showed strong CPL signals of opposite handedness depending on the cooling conditions, which originated from TATA locally-excited state (Figure 15 d-e). For each enantiomer, the fast and slow-cooled samples showed circularly polarized emission of similar intensities, with maximum recorded g_{lum} values of $+1.8\times10^{-2}$ and -1.7×10^{-2} for the (*S*) enantiomer, and -1.8×10^{-2} and $+1.5\times10^{-2}$ for the (*R*) enantiomer, respectively, being among the highest reported for supramolecular systems in solution. These finding demonstrate that the circularly polarized light of either handedness can be produced from the same enantiomer simply by controlling the temperature during its self-assembly process, a capability that stems from the hierarchical organization of the TATA core. This work introduces a new strategy for designing optically active materials, enabling precise control of CPL without altering molecular chirality-only assembly conditions.

An important challenge in the development of supramolecular polymers exhibiting CPL activity is the attainment of reproducible and highly controlled structural parameters, including dimensional precision and low dispersity, as these

View Article Online
DOI: 10.1039/D5SC07295B

govern the properties of the resulting materials. Furthermore, achieving this level of control in an aqueous medium would significantly broaden the scope of chiroptical applications, particularly within biologically relevant environments. In this regard, a proposal to precisely control the length and dispersity of supramolecular polymers with CPL activity in water would be to use living supramolecular polimerization (LSP) as George and coworkers proposes.[29] They designed two ethoxy-core-substituted naphthalene diimide (cNDI) appended with chiral dipeptide, referred as *L*-**26** and *D*-**26**, respectively (Figure 16a). These monomers can stack via π-stacking between the cNDI units, while the chiral peptide side chains promote intermolecular hydrogen bonding through their amide groups, leading to the formation of extended supramolecular polymers and imparting chirality to the cNDI core during the self-assembly. Additionally, the carboxylic acid groups engage in hydrogen bonding with water, enabling supramolecular polymerization in aqueous media. By exploiting pathway complexity, where monomers pass through monomeric (M), metastable (I), and thermodynamically stable (TS) states, the authors achieve kinetically controlled nucleation-elongation behaviour. Through temperature-dependent spectroscopy measurements, monomer, metastable and thermodynamically states were fully characterized. A sharp vibronic feature in absorption bands, absence of a CD signal and a narrow emission at 505 nm was observed for the monomeric of *L*-**26**. Upon fast-cooling, a slight red shift in absorption bands with an increased ratio between the vibronic bands at 365 and 346 nm with persistent absence of a CD signal and insignificant change in emission and excitation spectra suggested the presence of small aggregates, which was identified as metastable states (Figures 16b-d). Time-dependent absorption spectra exhibited a gradual red shift and broadening of the absorption band, accompanied by the appearance of a new absorption at ca. 510 nm. These changes indicate the evolution toward a thermodynamically stable self-assembled state, by the dynamic reorganization of monomers from its metastable phase (I) through extended intermolecular hydrogen bonding, which was also prove through bisignated CD spectrum centered at the π-π* and n-π* bands of cNDI evolved and a new characteristic band at ca 538 nm in the emission spectra, as is showed in Figure 16c. The resulting supramolecular polymers show strong chiroptical performance, with a notable CPL dissymmetry factor of 1.3×10^{-3} (Figure 16d). Moreover, seeding strategies varying seed concentration, monomer concentration and seed fragmentation via sonication were used to bypass nucleation and achieve highly efficient seeded growth, producing fibers with precisely tuneable lengths and very low dispersity. Multicycle seeding confirms living behaviour, enabling stepwise, length-controlled elongation. Overall, this work demonstrated one of the most efficient aqueous-phase LSP system reported, illustrating how LSP can be used to create functionally active, CPL-emitting supramolecular polymers with programmable structure-opening pathways for biological and optoelectronic applications.

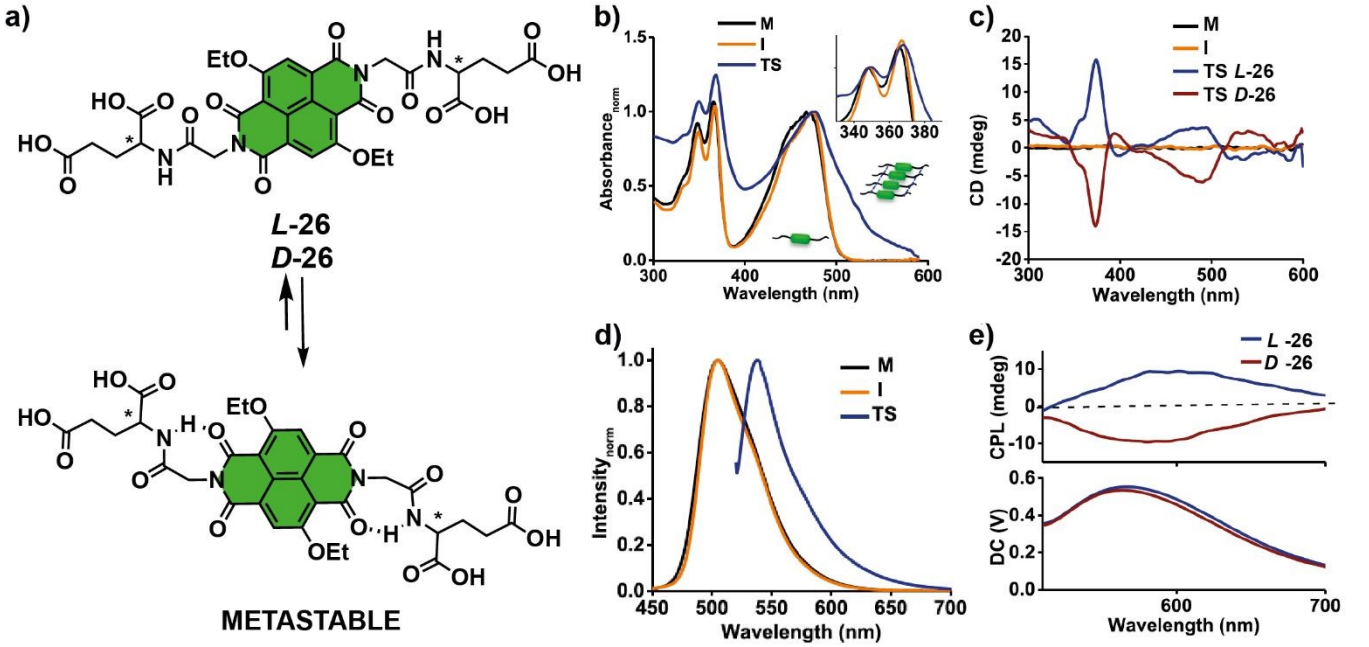

Fig. 16. (a) Structure of monomers ***L*-26** and ***D*-26**; Comparison of (b) normalized absorption (inset corresponds to zoomed in normalized absorption spectra at 346 nm); (c) CD spectra (Thermodynamically stable state, **TS**, state of both *L* and *D* isomers); (d) Normalized emission for Monomer (M), Metastable (**I**) and **TS** showing distinguished signals; (e) CPL and corresponding DC spectra of ***L*-26** and ***D*-26**. (Reproduced from reference 29 with permission from Wiley-VCH, copyright 2021)

Axial chirality in CPL-active supramolecular polymers.

In the last sections, we have seen that helical supramolecular polymers formed by the self-assembly of chiral scaffolds endowed with peripheral side chains decorated with stereogenic centres behave as CPL-active materials. However, in most of the reported examples of these chiral, CPL-active supramolecular polymers, the g_{lum} values are moderate. Since a major challenge faced by researchers in this field is to enhance the anisotropic g_{lum} factor, a valuable strategy consists in utilizing chiral scaffolds in which the asymmetry is present in the chromophore instead at the peripheral side chains. This strategy involves the self-assembly of chiral units exhibiting axial chirality, i. e., the asymmetry stemming from a chiral axis instead of a central carbon atom. Relevant examples of CPL-active supramolecular polymers in which the central aromatic core is endowed with helicenes, binaphthyls or *p*-cyclophanes have been reported in bibliography exhibiting remarkable anisotropy factors. In this section, we will review some of the most significant reports related to this strategy.

Despite helicenes, ortho-fused aromatic compounds yielding helical chirality,[30] have been extensively reported as efficient CPL-active systems,[31] much less studies have been published regarding CPL-active, helicene-based, supramolecular polymers. Probably, one of the first examples of CPL-active SPs was the phthalhydrazide-functionalized [7]helicene **27** reported by Takeuchi and coworkers in 2011 (Figure 17a). The two (*M*) and (*P)* enantiomers of **27** were separated by column chromatography on a chiral support. The enantioenriched (*M*)-[7]helicene **27** forms trimeric disks by the intermolecular H-bonding interaction between the phthalhydrazide units. These disks, due to the π-stacking of the [7]helicene cores, yield screw-shaped fibrous assemblies in toluene as solvent (Figure 17b). The SPs formed by the self-assembly of the enantioenriched *M* and *P* enantiomers displayed mirror image CPL spectra with outstanding g_{lum} values of 0.035 at the peak maxima.[32]

[5]Helicenes, decorated with two methyl groups at the 1 and 1' positions to prevent the racemization of the aromatic core and with imide units, have been reported to self-assemble into luminescent, spherical and uniform nanoparticles of 200 nm of diameter upon injecting a THF solution of the *M* or *P* enantioenriched tetrahydro[5]helicenes **28** into a water solution. These [5]helicenes **28** present different aryl groups at the 3 and 3' positions that allow modulating the colour emission (Figure 17). Interestingly, the co-assembly of [5]helicenes **(+)-*M*-28a**, **28d**, and **28e**, the three of them emitting separately in the blue, green and red region, affords white-emitting nanoparticles (Figures 17d and 17e).[33]

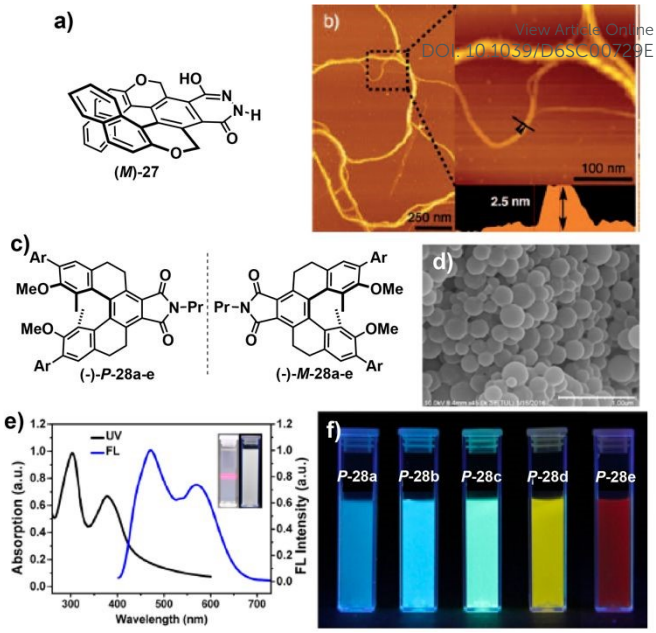

Fig. 17. (a) Chemical structure of the phthalhydrazide-functionalized [7]helicene **27**; (b) AFM images of (*M*)-**27** prepared in toluene (Reproduced from reference 30 with permission from Wiley-VCH, copyright 2011); c) Chemical structure of the *P* and *M* enantiomers of tetrahydro[5]helicenes **28**; SEM image (d) and UV−vis and fluorescence spectra (e) of the nanoparticles formed by the co-assembly of **(+)-*M*-28a, 28d,** and **28e** in water; the inset photographs in panel (d) are the images of nanoparticles under the naked eye and under 365 nm UV light irradiation; (f) Dispersion colours of the nanoparticles formed by [5]helicenes **28** under 365 nm excitation (panels 2d-f reproduced from reference 33 with permission from the American Chemical Society, copyright 2018).

[6]Helicenes are well-known scaffolds exhibiting not only exciting CPL-activity with outstanding g_{lum} values but also high values for B_{CPL}.[6b,34] Importantly, and unlike [5]helicenes, [6]helicenes possess a high racemization barrier that makes no necessary the decoration of the bay position of the helicene core to prevent the racemization of the corresponding *M* and *P* enantiomers of these helicenes.[30] We have reported on the formation of chiral SPs by using 2,15- and 4,13-disubstituted [6]helicenes endowed with peripheral benzamide units (compounds **29-32** in Figure 18a).[35] We have demonstrated that these series of [6]helicenes are molecularly dissolved in a good solvent like chloroform but in a non-polar solvent like methylcyclohexane (MCH) readily form chiral supramolecular polymers with rich chiroptical features. Interestingly, the substitution pattern of the [6]helicene core plays a crucial role in the self-assembling mode of the monomeric units and, consequently, in the chiroptical features. Thus, in the 2,15-disubstituted [6]helicenes **29** and **31**, the central aromatic core is not available for the π-stacking of the monomeric units and the intermolecular H-bonding interactions between the amide functional groups of the peripheral side chains results in a zig-zag arrangement of the chromophores (Figure 18b). On the contrary, in the 4,13-disubstituted [6]helicenes **30** and **32** the

central aromatic cores are more available for their π-stacking and the resulting SPs are formed by the synergy of both the intermolecular H-bonding interactions between the amide functional groups and the π-stacking of the aromatic backbones. The synergy of these non-covalent interactions results in a ladder-like arrangement of the monomeric units to give rise to the corresponding chiral supramolecular polymer (Figure 18b). To evaluate the stability of the supramolecular polymers formed by **29** and **30**, solvent denaturation (SD) experiments were performed by using mixtures of these helicenes in chloroform, a good solvent that provokes the disassembly of the SP, and in MCH, the poor solvent favouring the self-assembly.[36] Interestingly, the substitution pattern of the [6]helicene core plays a relevant role in the supramolecular polymerization mechanism of these two systems. Thus, whilst 2,15-disubstituted helicene **29** follows an isodesmic supramolecular polymerization mechanism, the 4,13-disubstituted helicene **30** is governed by a cooperative mechanism. The emission spectra of both enantiomers *M* and *P* of [6]helicene **29** in $CHCl_3$ show the characteristic vibronic structured photoluminescence (PL) of [6]helicenes[31] with three consecutive maxima at 430, 455, and 486 nm (λ_{exc} = 365 nm, φ = 0.35, and τ = 8.5 ns) (Figure 18d). This vibronic structure is also observed in the corresponding CPL spectrum that exhibit a remarkable dissymmetry factor g_{lum} with maximum values of +2.3/−2.6 × 10^{-2} (λ_{exc} = 365 nm) for **(*P*)-29** and **(*M*)-29**, respectively (Figure 18d). The emissive properties of the supramolecular polymers formed by these enantiomers in MCH also display very similar, but slightly red shifted, features with maxima at 436, 462, and 493 (λ_{exc} = 365 nm, φ = 0.59, and τ =12.2 ns). These maxima are also observed in the CPL spectra with maximum glum values of +2.0/−2.3 × 10^{-2} (λ_{exc} = 365 nm), respectively. These results demonstrate that the lack of π-stacking in the self-assembly of [6]helicenes **29** results in analogous values for the CPL activity of both the aggregated and non-aggregated states.[35a]

As in the previous example, the fluorescence spectra of **(*P*)-30** and **(*M*)-30** in $CHCl_3$ and MCH display the vibronic structured luminescence with the characteristic three consecutive maxima at around 430, 455 and 485 nm (Figure 18e). The substitution pattern of these [6]helicenes **30** plays a relevant role decreasing the g_{lum} values for both the monomeric species (−1.1/+1.3 × 10^{-3} for the *M* and *P* enantiomers, respectively, in $CHCl_3$, Figure 18e) and aggregated species (+1.4/−1.2 × 10^{-3}, for the *P* and *M* enantiomers, respectively, in MCH; Figure 18e). To our knowledge, this is the first observation of CPL sign inversion upon assembly in helicenes.[35a]

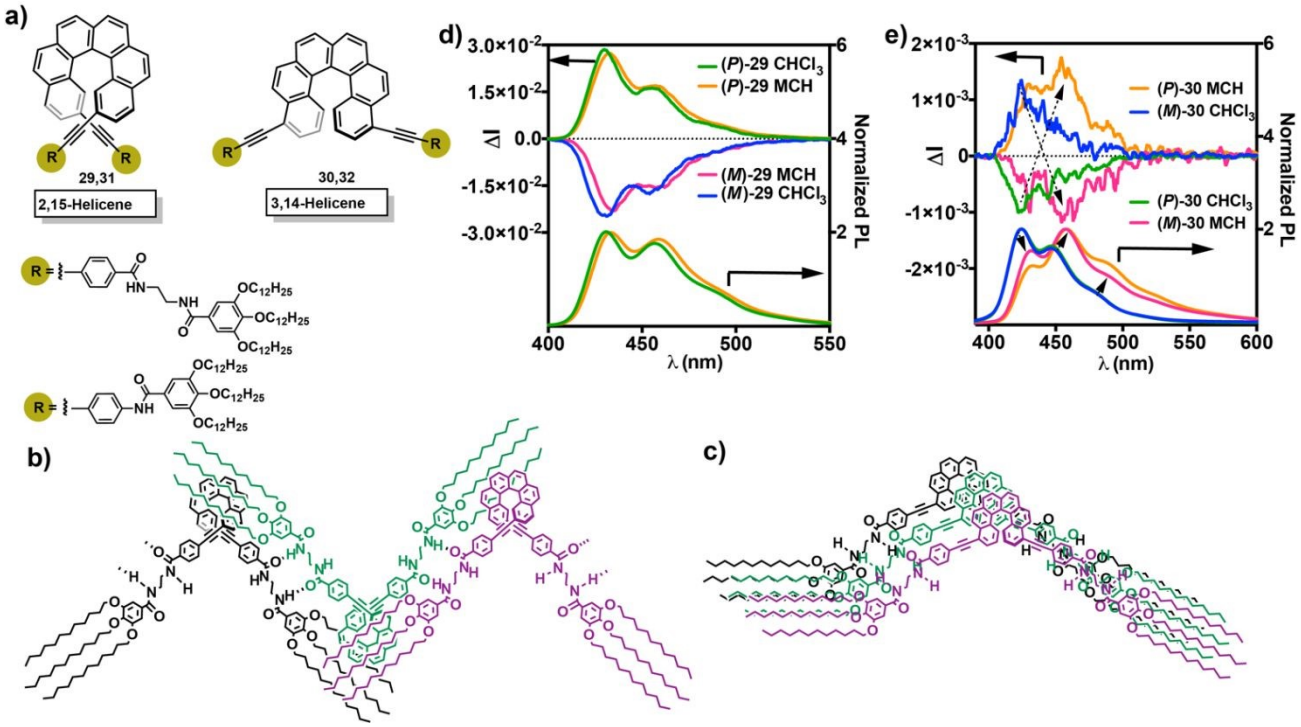

Fig. 18. (a) Chemical structure of the [6]helicenes **29-32**; (b) schematic illustration of the binding mode experienced by [6]helicenes **29-32** upon self-assembly; CPL/PL spectra of **(*P*)-29** and **(*M*)-29** (d) and **(*P*)-30** and **(*M*)-30** (e) in monomeric and aggregated states ($CHCl_3$ and MCH, respectively) (Reproduced from reference 35 with permission from American Chemical Society, copyright 2022).

The presence of only one amide functional group per branch in [6]helicenes **31** and **32** reduces notably the stability of the aggregated species formed by these helicenes. However, the 2,15- and 4,13-substitution pattern result in a similar zigzag and ladder-like arrangement of the monomeric units in the corresponding aggregated species formed by **31** and **32**, respectively. In these helicenes, the CPL activity of both monomeric and aggregated species is very similar to those recorded for compounds **29** and **30** with g_{lum} values of +2.8/-2.6×10^{-2} for **31** and +2.0/-2.0×10^{-3} for **32**. It is worth mentioning

View Article Online
DOI: 10.1039/D6SC00729E

that in this case, and unlike to those observed for [6]helicene **30**, the CPL of both the monomeric and aggregated states of **32** display the same sign.[35b]

We have already seen that a common strategy to improve the emission of supramolecular polymers consists in utilizing non-planar aromatic units that, through an AIE effect, experience an increase in the emission intensity. This AIE phenomenon has been also utilized in CPL-active supramolecular polymers in which the monomeric species are decorated with point chirality in the peripheral side chains as we have already seen in the previous section.[22] With this idea in mind, the previously mentioned 2,15- and 4,13-disubstituted [6]helicene cores have been functionalized with cyanostilbene moieties (compounds **33**, Figure 19a). The resulting [6]helicene monomeric species readily form chiral supramolecular polymers in non-polar MCH following a cooperative mechanism regardless the substitution pattern. Despite the clear increase of the emission intensity upon aggregation (Figures 19b and 19c), the CPL activity of the corresponding chiral supramolecular polymers of **33** is similar to that registered for [6]helicenes **30** and **32** with g_{lum} values of around +2/-2 x 10^{-3} for each enantiomer (Figures 19d and 19e). The presence of the cyanostilbene moieties in the 2,15-disubstituted [6]helicene **33a** present lower values of g_{lum} than that reported for [6]helicenes **29** and **31** (Figures 19d and 19e).[37] Despite the relatively low g_{lum} values, the remarkable AIE effect observed upon self-assembly results in better B_{CPL}. This parameter increases from values of 2.8 and 5.4 for the monomeric species to 11.6 and 40.6 for **33a** and **33b**, respectively.[37] The restricted rotation around the single bond connecting two aromatic rings makes biaryl-based compounds excellent chiral scaffolds for inducing stereoselectivity in various applications and, additionally, to achieve CPL-active systems.[38,39]

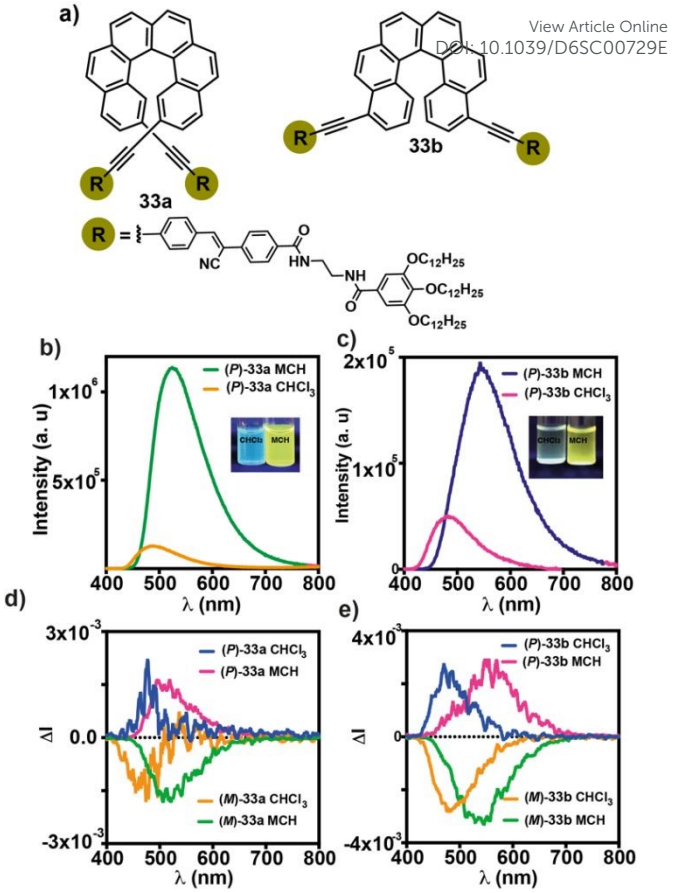

Fig. 19. (a) Chemical structure of the [6]helicenes **33**; Emission spectra of **(*M*)-33a** (b) and **(*M*)-33b** (c); CPL spectra of **(*M*)-33a**, **(*P*)-33a** (d) and **(*M*)-33b** and **(*P*)-33b** (e) $CHCl_3$ and MCH, respectively. The inset in panels (b) and (c) show the pictures of the solutions of **(*M*)-33a** (b) and **(*M*)-33b** in $CHCl_3$ and MCH upon excitation at λ = 365 nm. (Reproduced from reference 37 with permission from Royal Society of Chemistry, copyright 2024).

Enantioenriched biaryl-based compounds have been also utilized as monomeric units to attain chiral supramolecular polymers displaying a CPL-activity for the aggregated species different than that registered for the monomeric species. To the best of our knowledge, one of the first examples of CPL-active supramolecular polymers endowed with biaryl units was reported by Kumar, Nakashima, Tsumatori and Kawai in 2014. In these CPL-active supramolecular polymers (compounds **34** in Figure 20a), an enantioenriched binaphthalene core, *R or S,* was decorated with two asymmetrically substituted perylenediimide (PDIs) units, a highly utilized chromophore to build up supramolecular polymers with exciting optical and chiroptical properties,[40] that self-assemble into nanoparticles or 1D supramolecular polymers depending on the concentration range or the solvent utilized to form the corresponding supramolecular ensembles (Figure 20a). The presence of the chiral binaphthalene core of compounds **34** results in a clear chiroptical response for the molecularly dissolved monomeric species, registered in $CHCl_3$ and a total concentration of 10 μM with a g_{lum} ~ 0.003. Increasing the

concentration of these chromophores to 3 mM in $CHCl_3$ yields uniform nanoparticles with diameters of 26 nm and values for g_{lum} up to 0.008 that implies the contribution of the chiral aggregates to the enhanced fluorescence dissymmetry. On the other hand, using a mixture MCH/$CHCl_3$ 19/1 as solvent, provokes an efficient supramolecular polymerization of these PDI-based systems **34** that yields H-type aggregates showing a rope-like morphology. Furthermore, a noticeable increase in the g_{lum} values of 0.018. It is worth mentioning that in this solvent mixture, and unlike that observed in $CHCl_3$, the g_{lum} values remain unaltered upon increasing the concentration (Figure 20b).[41] Shortly after these studies, the authors performed a majority rules experiment in which both enantiomers **(*S*)-34** and **(*R*)-34** were mixed at different ratio but keeping constant the total concentration. These MRs experiment demonstrate that the morphology of the aggregates range from nanoparticles for the racemic mixture of both enantiomers to fibrillar supramolecular polymers. Furthermore, the g_{lum} values were cancelled for the racemic mixture but increases up to 0.02 when one of the enantiomers were in excess in the mixture.[42]

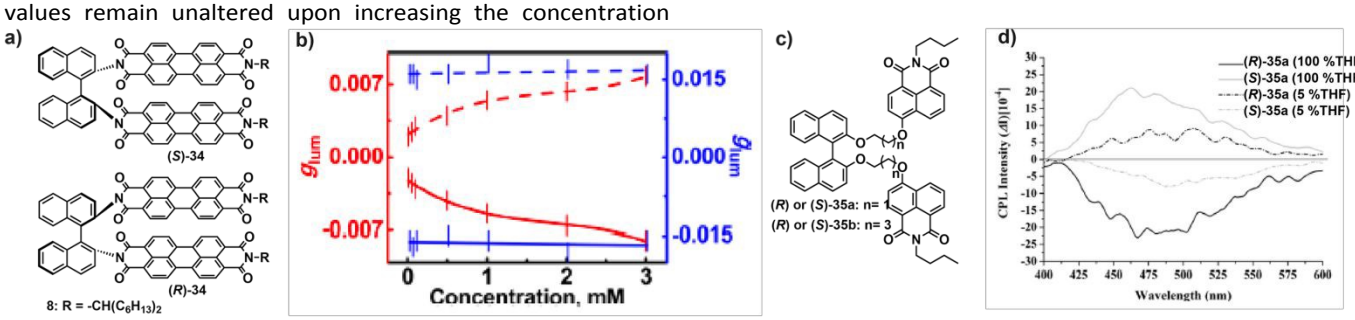

Fig. 20. (a) Chemical structure of the binaphthalene derivatives **34**; (b) plot of g_{lum} vs. concentration for *R* (solid lines) and *S* (broken lines) enantiomers of **34** in $CHCl_3$ (red traces) and a mixture (1:19) of $CHCl_3$/MCH (blue traces). (Reproduced from reference 41 with permission from American Chemical Society, copyright 2014); (c) chemical structure of the chiral monoimides **35**; (d) CPL spectra of **35a** in THF and 5:95 (v/v) THF/H_2O mixtures (Reproduced from reference 43 with permission from Wiley-VCH, copyright 2015)

The decoration of enantioenriched binaphthalene cores with luminescent monoimides has been reported by Zhang, Zhu, Cheng and coworkers to invert the CPL activity of the resulting chiral, luminescent systems **35** when the monomeric species self-assemble upon adding increasing amounts of water (Figure 20c). The studies performed with these chiral monoimides demonstrate that the CPL-activity is barely modified upon increasing the tether connecting both the binaphthalene and the monoamide units. However, the addition of water provokes a clear increase in the g_{lum} values due to the formation of aggregated species in which the dihedral angle of the binaphthalene core decreases upon aggregation (Figure 20d).[43] A similar strategy has been followed by Balasubramanian, George and coworkers to achieve tuneable excimeric CPL spanning the visible range, with remarkable values of g_{lum} in the range of 0.015. These values of g_{lum} have been obtained upon self-assembly of a chiral binaphthalene decorated with two naphthalenediimides (NDIs) **36** that, in turn, have been modified by attaching two electron-donating ethoxy groups. Whilst the monomeric species do not exhibit any CPL activity, the aggregates formed in mixtures tetrachloroethane (TCE) and MCH show an intense CPL activity and CPL brightness (Figure 21a).[44]

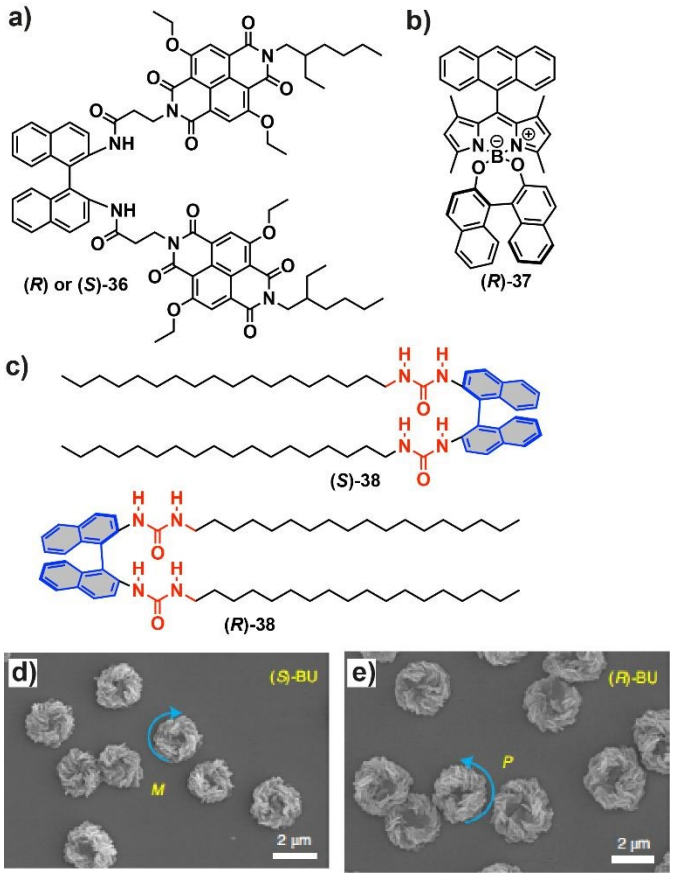

Fig. 21. Chemical structure of the binaphthalene derivatives **36** (a), **37** (b) and **38** (c); SEM images of the chiral toroids formed upon self-assembly of **(*S*)-38** (d) and **(*R*)-38** (e) (Reproduced

from reference 46 CC BY-NC-ND with permission from Springer, copyright 2012)

The synergy of the asymmetry of a binaphthalene core, the ability to self-assemble of an anthracene moiety and the narrow-band emissive properties of the BODIPY has been harnessed to prepare the CPL-active monomeric scaffold **37** that self-assembles in a THF/H_2O mixture giving rise initially to an AIE phenomenon that experiences a light-triggered transition yielding an aggregation caused quenching (ACQ) with high g_{lum} values of 0.048, one of the highest values reported for CPL-active supramolecular polymers (Figure 21b).[45] The decoration of chiral binaphthalenes with urea moieties has allowed to Ouyang, Liu and coworkers to prepare helical toroids upon the hierarchical self-assembly of chiral compounds **38** (Figure 21c). A drop-evaporation assembly protocol on a solid substrate from pre-assembled intermediate colloids of enantioenriched binaphthalene bisurea **38** leads to microtoroids with preferred helicity due to the operation of H-bonds between the ureas and the π-stacking of the binaphthalene units (Figure 21d,e). The molecular asymmetry embedded in the starting binaphthalenes conditions the final chirality of the toroidal aggregates. The chiral nature of these toroids results in a rich chiroptical response and the formation of CPL-active systems with g_{lum} values of 0.002.[46]

The self-assembly of chiral scaffolds to yield supramolecular polymers is very often accompanied by the formation of excimers that can diminish the CPL-activity of such aggregated species due to the luminescence quenching. A sharp strategy to cancel the excimer emission thus increasing the CPL-activity consists in the formation of charge transfer (CT) complexes between chiral emissive arenes, acting as electron-donating segments, and different electron-withdrawing, achiral, small molecules like tetracyanobenzene (TCNB). In these reports, the chiral, emissive, electron-donating system is a derivative of the (*S*) or the (*R*) enantiomer of the octahydrobinaphthalene endowed with pyrene (compound **39** in Figure 22) or anthracene (compound **40** in Figure 22). Whilst chiral **39** readily forms non-emissive CT-complexes with electron-withdrawing molecules like tetrafluoro-*p*-benzoquinone, tetracyanoethylene or tetracyano-*p*-quinodimethane, the CT-complex formed by mixing **39** and TCNB results in a reddish, highly emissive species that, in addition, present a remarkable CPL-activity showing g_{lum} values of 0.017.[47] This strategy has been extended to octafluoronaphthalene (**OFN**). This electron-withdrawing system forms highly emissive CT-complexes with both chiral **39** and **40** due to the complementary arene-perfluoroarene interactions (Figure 22). These emissive CT-complexes also present a remarkable CPL-activity with g_{lum} values of ~10^{-3}, one order of magnitude larger than that registered for the monomeric species.[48]

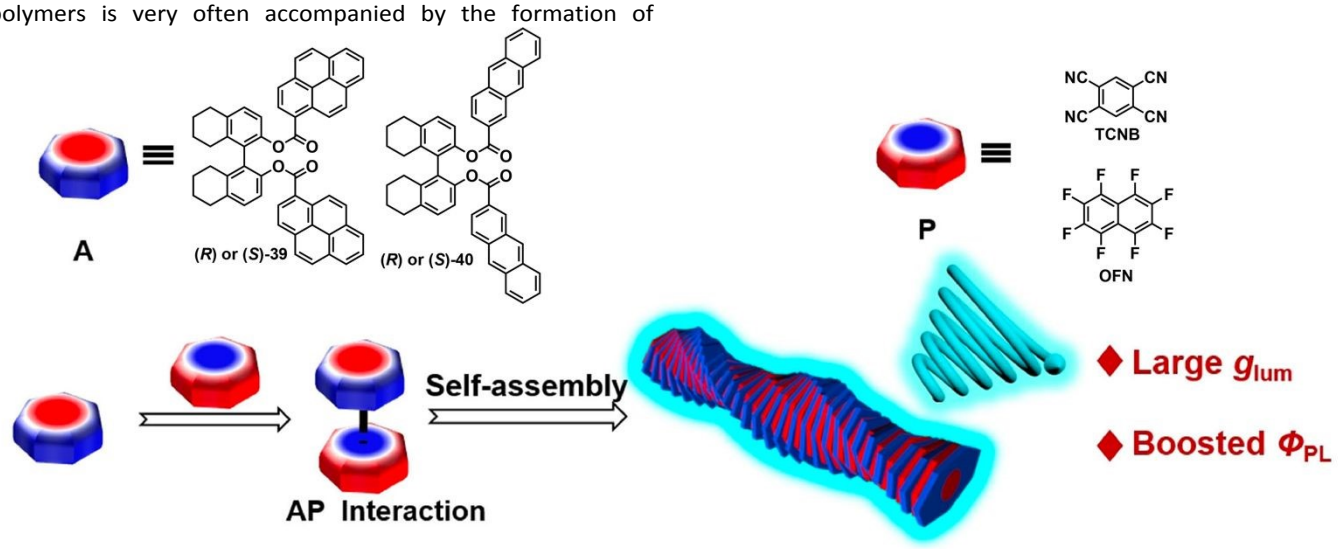

Fig. 22. Arene-perfluoroarene interaction between chiral π donors **39** or **40** and achiral π acceptors TCNB or OFN. (Reproduced from reference 48 with permission from Wiley-VCH, copyright 2021)

Applications of CPL-active supramolecular polymers

In addition to the basic studies necessary to shed light on the achievement of efficient CPL-active supramolecular polymers, the most relevant issue for these materials is their application in different fields and, very especially, in the fabrication of circularly polarized organic light-emitting diodes (CP-OLEDs) and sensing technologies. Upon reviewing basic aspects on CPL-active supramolecular polymers and the different families of compounds able to show this relevant characteristic, this part of the review will collect some of the applications reported in literature regarding the fabrication of optoelectronic devices. Circular polarizers are widely employed in OLEDs to improve image contrast by reducing ambient reflectivity, but they attenuate nearly half of the emitted light, causing brightness loss and higher energy consumption. CP-OLEDs that emit circularly polarized light matching the polarizer's handedness can avoid this inefficiency.[49] The first CP-OLEDs reported in the literature were fabricated by utilizing chiral, covalent polymers like a chiral oligo(phenylenevinylene) or polyfluorene.[50] The

View Article Online
DOI: 10.1039/D4SC00720E

incorporation of metal complexes like Eu(III), Ir(III) or Pt(II) allows the fabrication of semitransparent devices with relatively high circularly polarized electroluminescence signal with high g_{EL} up to -0.38 but still low efficiencies.[51] The incorporation of self-assembled structures has allowed to reach better CP-OLED efficiencies. Thus, Cheng and coworkers fabricated a device in which the active layer was prepared by a combination of a chiral dihydropyridine **41a** and an achiral monoamide endowed with a triphenylamine moiety **41b** in which the former transfer its asymmetry to the latter and the resulting aggregates, upon annealing, present a strong CPL signal. The multisandwich device prepared from the helical aggregates generated upon mixing both **41a** and **41b** exhibited strong brightness, good luminous efficiency, and a high g_{EL} value of 0.023 (Figure 23a).[52]

Very recently, Meijer, Friend and coworkers have reported on the fabrication of an CP-OLED utilizing the chiral triazatruxene **42** that self-assembles into helical aggregates (Figure 23b). Cosublimation of **42** as a guest within a structurally mismatched host, constituted by a mixture of the hole transporting 4,4'-bis(*N*-carbazolyl)-1,1'-biphenyl or the ambipolar 3',5'-di(carbazol-9-yl)-[1,1'-biphenyl]-3,5-dicarbonitrile, enabled the formation of thin films in which chiral crystallization occurred in situ via thermally induced nanophase segregation of the dopant and host, while maintaining film integrity. The resulting OLEDs exhibited external quantum efficiencies up to 16% and electroluminescence dissymmetries ≥10% and values of 0.1 for g_{EL}.[53]

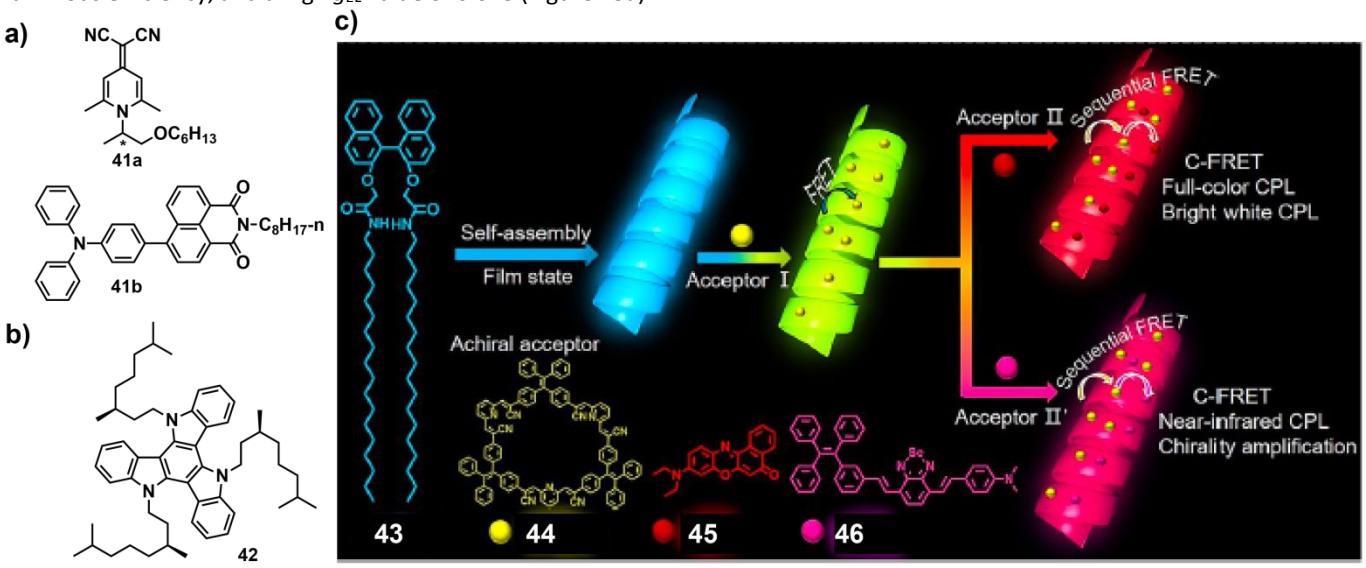

Fig. 23. Chemical structure of the dihydropyridine **41a**, the monoamide **41b** (a) and the triazatruxene **42** (b); (c) Schematic illustration of the process of chiral light harvesting and full-colour circularly polarized luminescence. In this system, **43** functioned as an initiator of chirality, **44** served as a conveyor, **45**-**46** were the terminal acceptors. (Reproduced from reference 54 with permission from American Chemical Society, copyright 2022).

Zang et al. developed a chiral light-harvesting system (CLHS) based on sequential circularly polarized fluorescence resonance energy transfer (C-FRET) by integrating a chiral, light-absorbing initiator (**43**) with TPE-based macrocycles (**44**) exhibiting AIE, along with red and near-infrared emissive dyes (**45**-**46**). This design enabled continuous chirality transmission and amplification in conjunction with efficient energy transfer. In this system, a pair of the chiral binaphthalene **43**, capable of self-assembling into helical nanostructures, was employed as the primary donor. Supramolecular assembly facilitated the successful incorporation of three energy acceptors **44**-**46** into the helical framework, producing a CLHS with tuneable fluorescence colours and stepwise energy and chiral transfer. The resulting system exhibited a maximum g_{lum} value of 0.035. Further studies revealed that efficient energy transfer was promoted by the close spatial proximity between donors and acceptors and their substantial spectral overlap. Moreover, the rigid cavity of the green-emitting AIE macrocycle **44**, together with hierarchical host–guest interactions, enabled the chirality of the supramolecular synthons **43** to be continuously transferred and even amplified in the otherwise achiral dye molecules **45**-**46**. By optimizing the component ratios, the authors achieved an energy transfer efficiency of up to 98.5%, a fluorescence quantum yield of 37%, g_{lum} value of 0.035, CPL with tuneable emission colours, and CPL emission approaching CIE standard white light across a broad spectral range (360–800 nm) (Figure 23e).[54]

Finally, conventional methods such as barcodes, watermarks, and QR codes have become easy to replicate which makes advanced anticounterfeiting technologies necessary. Chiroptical anticounterfeiting has emerged as a promising next-generation solution due to its multiple emission characteristics, including intensity, wavelength, lifetime, and chirality. Central to this approach is the development of CPL systems with high g□ᵤ□ values. Exciting anticounterfeiting effect has been reported by using CPL-active systems like a luminescent spiropyran and Zn^{2+} [55] or nematic liquid crystals and photoswitches based on diarylethenes.[56] These seminal reports have complemented with the anticounterfeiting effect described by Zhang, Qu, Liu and coworkers for the

View Article Online
DOI: 10.1039/D5SC07805E

supramolecular polymers formed by the homochiral metallosupramolecular polymer formed by a cholesteric-appended Schiff base ligands upon complexation with Zn^{2+} cations (compound **3** in Figure 24a). The self-assembly of the resulting complexes can form different aggregates with different morphologies and CPL-activity that changes with time. These kinetic changes, involving CPL-inversion and fluorescence colour switching, have been harnessed to encrypt information. To illustrate this effect, two different experiments have been carried out. In the first of these experiments a tulip flower with the complex **3**·Zn^{2+} exhibited a time dependent fluorescence transition from cyan to blue within 60 seconds (Figure 24b). In the second experiment, a display able to generate QR was built up with two inks, Ink 1, that remains inert (no readable information), and Ink 2, containing the **3**·Zn^{2+} complex that gradually reveals the encoded data over time, representing an active or "enabled" state. The changes of the supramolecular polymers formed by the **3**·Zn^{2+} complex provokes the emission changes that reveals the complete QR code (Figure 24c).[17a] These applications of CPL-active supramolecular polymers exemplify the outstanding future for these chiral aggregated species.

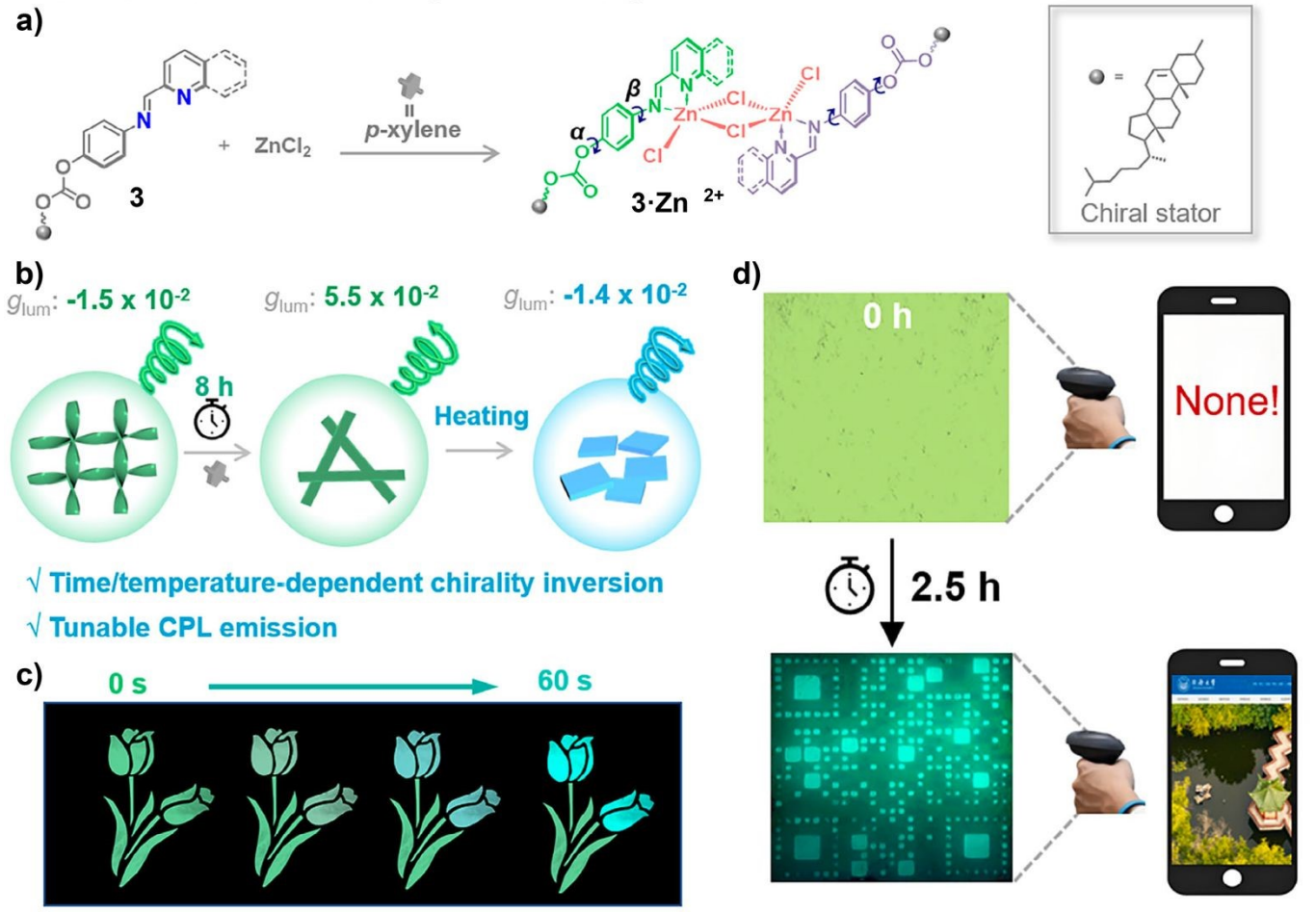

Fig. 24. (a) Chemical structure of the complexes formed by the Schiff bases **3** and Zn^{2+}; (b) Schematic illustration of the conformation transformation inducing dynamic multiple chirality inversion and tuneable CPL; (c) and (d) Design principle of time-dependent information encryption: (c) Solid-state material demonstration of fluorescence changes in response to time and temperature of **3**·Zn^{2+} complex aggregates at 385 K; (c) Solid-state material demonstration of completely spontaneous time-dependent fluorescence changes of **3**·Zn^{2+} complex aggregates and the application in dynamic QR code display (Reproduced from reference 17a with permission from Wiley-VCH, copyright 2025)

Conclusions

The research field of supramolecular polymers is highly active, with systems of ever-increasing complexity continually being developed. Mathematical models designed to study SP formation have played a key role in uncovering new approaches and functionalities for these self- or co-assembled supramolecular species. Within this broad field, chiral SPs represent a particularly valuable benchmark, as they enable the generation of helical structures that can model the origin of homochirality in nature and give rise to other compelling functionalities. Intriguingly, the presence in the monomeric units constitutive of such chiral SPs of emissive moieties can yield emissive aggregated species that, in addition, can behave as CPL-active species. This property confers chiral SPs of an additional interest in different research fields and applications.

In this review, we highlight relevant examples of the different strategies utilized to achieve CPL-active supramolecular polymers. These strategies encompass the decoration of the monomeric units of elements of asymmetry (point or axial chirality) and the presence of metallic species. In all the examples of CPL-active supramolecular polymers collected in this review the influence of light, solvent, temperature and so forth as external stimuli demonstrates the versatility of these supramolecular systems to afford CPL-active systems with remarkable values for the dissymmetry factor g_{lum} and the CPL brightness B_{CPL}. A number of examples of CPL-active metallo-organic SPs as well as purely organic systems is collected together with outstanding applications of such CPL-active SPs as active layer in optoelectronic devices, anticounterfeiting and encryption.

Author contributions

Carmen Atienza and Fátima García, visualization, investigation and writing-original draft, review; Luis Sánchez, conceptualization, supervision, writing-original draft, review.

Conflicts of interest

There are no conflicts to declare.

Data availability

No primary research results, software or code have been included, and no new data were generated or analysed as part of this review

Acknowledgements

Financial support by the MCIN/AEI of Spain (PID2023-146971NB-I00) is acknowledged

Notes and references

1 Relevant reviews on supramolecular polymers: a) L. Brunsveld, B. J. B. Folmer, E. W. Meijer and R. P. Sijbesma, *Chem. Rev.*, 2001, **101**, 4071; b) M. Wehner and F. Würthner, *Nat. Rev.*, 2019, **4**, 38; c) L. Yang, X. Tan, Z. Wang and X. Zhang, *Chem. Rev.*, 2015, **115**, 7196.

2 a) T. Aida, A. Takemura, M. Fuse and S. Inoue, *J. Chem. Soc. Chem. Commun.*, **1988**, *5*, 391; b) C. Fouquey, J.-M. Lehn and A.-M. Levelut, *Adv. Mater.*, 1990, **2**, 254; c) R. P. Sijbesma, F. H. Beijer, L. Brunsveld, B. J. B. Folmer, J. H. K. K. Hirschberg, R. F. M. Lange, J. K. L. Lowe and E. W. Meijer, *Science*, 1997, **278**, 1601.

3 a) T. Aida, E. W. Meijer and S. I. Stupp, *Science*, 2012, **335**, 813; b) Z. Alvarez, A. N. Kolberg-Edelbrock, I. R. Sasselli, J. A. Ortega, R. Qiu, Z. Syrgiannis, P. A. Mirau, F. Chen, S. M. Chin, S. Weigand, E. Kiskinis and S. I. Stupp, *Science*, 2021, **374**, 848; c) O. Dumele, L. Đordevic, H. Sai, T. J. Cotey, M. H. Sangji, K. Sato, A. J. Dannenhoffer and S. I. Stupp, *J. Am. Chem. Soc.*, 2022, **144**, 3127; d) W. Zhao, J. Tropp, B. Qiao, M. Pink, J. D. Azoulay and A. H. Flood, *J. Am. Chem. Soc.*, 2020, **142**, 2579; e) Y. Yanagisawa, Y. Nan, K. Okuro and T. Aida, *Science*, 2018, **359**, 72; f) Y. Yamamoto, T. Fukushima, Y. Suna, N. Ishii, A. Saeki, S. Seki, S. Tagawa, M. Taniguchi, T. Kawai and T. Aida, *Science*, 2006, **314**, 1761; g) R. Chen, A. Hammoud, P. Aoun, M. A. Martínez-Aguirre, N. Vanthuyne, R. Maruchenko, P. Brocorens, L. Bouteiller and M. Raynal, *Nat. Commun.*, 2024, **15**, 4116.

4 a) A. R. A. Palmans and E. W. Meijer, *Angew. Chem. Int. Ed.*, 2007, **46**, 8948; b) F. García, R. Gómez and L. Sánchez, *Chem. Soc. Rev.*, 2023, **52**, 7524.

5 J. P. Riehl and F. S. Richardson, *Chem. Rev,* **86**, 1.

6 a) H. Tanaka, Y. Inoue and T. Mori, *ChemPhotoChem* 2018, **2**, 386; b) B. Doistau, J-R Jiménez and C. Piguet (2020) *Front. Chem.* 2020, **8**, 555. c) Arrico, L. Di Bari and F. Zinna, *Chem. Eur. J.*, 2021, **27**, 2920.

7 K.-L. Wong, J.-C. G. Bünzli and P. A. Tanner, *J. Lumin.*, 2020, **224**, 117256.

8 C. A. Emeis and L. J. Oosterhoff, *Chem. Phys. Lett.*, 1967, **1**, 129.

9 Y. Chen, *Mater. Today Chem.*, 2022, **23**, 100651.

10 a) J. Kumar, T. Nakashima and T. Kawai, *J. Phys. Chem. Lett.*, 2015, **6**, 3445; b) H. Yan, Y. He, D. Wang, T. Han and B. Z. Tang, *Aggregate*, 2023, **4**, e331.

11 a) Y. Sang, J. Han, T. Zhao, P. Duan and M. Liu, *Adv. Mater.*, 2020, **32**, 1900110; b) R. D. Mukhopadhyay and A. Ajayaghosh, *Chem. Soc. Rev.*, 2023, **52**, 8635.

12 S. Datta, H. Itabashi, T. Saitoand S. Yagai, *Nat. Chem.* 2025, **17**, 477.

13 Y. D. Karmakar, P. Khanra, B. Ghosh, L. Roy and A. Das, *Small,* 2026, e12262.

14 a) L. A. Estroff and A. D. Hamailton, *Chem. Rev.* 2004, **104**, 1201. b) N. M. Sangeetha and U. Maitra, *Chem. Soc. Rev.* 2005, **34**, 821. c) J. L. Lunkley, D. Shirotani, K. Yamanari, S. Kaizaki and G. Muller, *J. Am. Chem. Soc.*, 2008, **130**, 13814. d) F. Zinna, U. Giovanella and L. Di Bari, *Adv. Mater.* 2015, **27**, 1791. e) T. Ikeda, M. Takayama, J. Kumar, T. Kawai and T. Haino, *Dalton. Trans.*, 2015, **44**, 1356. f) Y. B. Tan, Y. Okayasu, S. Katao, Y. Nishikawa, F. Asanoma, M. Yamada, J. Yuasa and T. Kawai, *J. Am. Chem. Soc.*, 2020, **142**, 17653. g) X.-Y. Luo and M. Pan, Coord. Chem. Rev., 2022, 468, 21640. h) M. Tsurui, R. Takizawa, Y. Kitagawa, M. Wang, M. Kobayashi, T. Taketsugu and Y. Hasegawa, *Angew. Chem., Int. Ed.*, 2024, **63**, e202405584.

15 D. Niu, Y. Jiang, L. Ji, G. Ouyang and M. Liu, *Angew. Chem. Int. Ed.* 2019, **58**, 5946.

16 a) G. Liu, J. Sheng, W. L. Teo, G. Yang, H. Wu, Y. Li and Y. Zhao, *J. Am. Chem. Soc.* 2018, **140**, 16275; b) K. Fu and G. Liu, *Chem. Commun.*, 2023, **59**, 13751; c) L. Yao, K. Fu, X. Wang, M. He, W. Zhang, P.-Y. Liu, Y. P. He and G. Liu, *ACS Nano* 2023, **17**, 2159; d) K. Fu, D.-H. Qu and G. Liu, *J. Am. Chem. Soc.* 2024, **146**, 33832.

17 a) M. He, P. Chen, Q. Wang, S. Zheng, C. Zhang, D.-H. Qu and G. Liu, *Adv. Funct. Mater.* 2025, e10772; b) M. He, H. Su, L. Zhu and G. Liu *Chem. Mater.* 2024, **36**, 2508.

18 G. Zou, Z. Jiang, D. Li, Q. Li and Y. Cheng, *Chem. Sci.* 2024, **15**, 18534.

19 X. Niu, X. Ou, S. Ren, K. Wang, F. Song, X. Dong, W.-J. Guo, H.-Q. Peng, Z. Zhao, J. W. Y. Lam, Y. S. Zhao, F. Li, S.-Y. Yu and B. Z. Tang, *Aggregate.* 2025, **6**, e70003.

20 A. Gopal, M. Hifsudheen, S. Furimi, M. Takeuchi and A. Ajayaghosh, *Angew. Chem. Int. Ed.* 2012, **51**, 1.

21 J. Kumar, T. Nakashima, H. Tsumatori, M. Mori, M. Naito and T. Kawai, *Chem. Eur. J.* 2013, **19**, 14090.

22 L. López-Gandul, C. Naranjo, C. Sánchez, R. Rodríguez, R. Gómez, J. Crassous and L. Sánchez, *Chem. Sci.* 2022, **13**, 11577.

23 Y. Xue, C. Zhang, T. Lv, L. Qiu and F. Wang, *Angew. Chem. Int. Ed.* 2023, **62**, e202300972.

DOI: 10.1039/D6SC00729E

24 a) X. Shang, I. Song, H. Ohtsu, Y. H. Lee, T. Zhao, T. Kojima, J. H. Jun, M. Kawano and J. H. Oh, *Adv. Mater.* 2017, **29**, 1605828; b) M. Schulz, F. Balzer, D. Scheunemann, O. Arteaga, A. Lützen, S. C. J. Meskers and M. Schiek, *Adv. Funct. Mater.* 2019, **29**, 1900684; c) X. Shang, I. Song, J. H. Lee, W. Choi, J. Ahn, H. Ohtsu, J. C. Kim, J. Y. Koo, S. K. Kwak and J. H. Oh, *ACS Nano* 2020, **14**, 14146-14156; d) L. Liu, Y. Yang, Y. Wang, M. A. Adil, Y. Zhao, J. Zhang, K. Chen, D. Deng, H. Zhang, K. Amin, Y. Wu, Y. Zhang and Z. Wei, *ACS Mater. Lett.* 2022, **4**, 401.

25 W. Yuan, L. Chen, Ch. Yuan, Z. Zhang, X. Chen, X. Zhang, J. Guo, Ch. Qian, Z. Zhao and Y. Zhao, *Nat. Commun.* 2023, **14**, 8022.

26 L. Gao, R. Liao, L. Ao, Y. Zhang, J. Jin and F. Wang, *Angew. Chem. Int. Ed.* 2025*,* **64***,* e202505776.

27 Y. Guo, Y. Zhan, J. Ma, R. Liao and F. Wang, *Nat. Commun.* 2024, **15**, 9303.

28 T.-A. Cucuiet, A. Vargas Jentzsch, F. Picini, M. Maaloum, G. Raffy, E. Moulin, D. M. Bassani and N. Giuseppone, *Angew. Chem. Int. Ed.* 2025, e202516824.

29 S. Patra, S. Dhiman and S. J. George, *Chem. Mater.* 2024, **36**, 9460.

30 a) J. Crassous, I. G. Stará and I. Starý, Helicenes - Synthesis, Properties and Applications, Wiley, 2022; b) C.-F. Chen and Y. Shen, in Helicene Chemistry: From Synthesis to Applications, Springer: Berlin, Heidelberg, 2017; c) M. Gingras, *Chem. Soc. Rev.* 2013, **42**, 968; d) Y. Shen and C.-F. Chen, *Chem. Rev*. 2012, **112**, 1463; e) K. Dhbaibi, L. Favereau and J. Crassous, *Chem. Rev.* 2019, **119**, 8846.

31 a) K. Dhbaibi, L. Abella, S. Meunier-Della-Gatta, T. Roisnel, N. Vanthuyne, B. Jamoussi, G. Pieters, B. Racine, E. Quesnel, J. Autschbach, J. Crassous and L. Favereau, *Chem. Sci.* 2021, **12**, 5522; b) M. J. Narcis and N. Takenaka, *Eur. J. Org. Chem*. 2014, 21; c) D. Schweinfurth, M. Zalibera, M. Kathan, C. Shen, M. Mazzolini, N. Trapp, J. Crassous, G. Gescheidt and F. Diederich, *J. Am. Chem. Soc.* 2014, **136**, 13045; d) E. Anger, M. Srebro, N. Vanthuyne, L. Toupet, S. Rigaut, C. Roussel, J. Autschbach, J. Crassous and R. Réau, *J. Am. Chem. Soc.* 2012, **134**, 15628; e) T. Verbiest, S. V. Elshocht, M. Kauranen, L. Hellemans, J. Snauwaert, C. Nuckolls, T. J. Katz and A. Persoons, *Science* 1998, **282**, 913.

32 T. Kaseyama, S. Furumi, X. Zhang, K. Tanaka and M. Takeuchi, *Angew. Chem. Int. Ed.,* 2011, **50**, 3684.

33 M. Li, C. Zhang, L. Fang, L. Shi, Z. Tang, H.-Y. Lu and C.-F. Chen, *ACS Appl. Mater. Interfaces* 2018, **10**, 8225.

34 C. Shen, F. Gan, G. Zhang, Y. Ding, J. Wang, R. Wang, J. Crassous and H. Qiu, *Mater. Chem. Front.,* 2020, **4**, 837.

35 (a) R. Rodríguez, C. Naranjo, A. Kumar, P. Matozzo, T. Kumar Das, Q. Zhu, N. Vanthuyne, R. Gómez, R. Naaman, L. Sánchez and J. Crassous, *J. Am. Chem. Soc.,* 2022, **144**, 7709; (b) R. Rodríguez, C. Naranjo, A. Kumar, K. Dhbaibi, P. Matozzo, F. Camerel, N. Vanthuyne, R. Gómez, R. Naaman, L. Sánchez and J. Crassous, *Chem. –Eur. J*., 2023, **29**, e202302254.

36 P. A. Korevaar, C. Schaefer, T. F. A. de Greef and E. W. Meijer, *J. Am. Chem. Soc*., 2012, **134**, 13482.

37 L. López-Gandul, R. Rodríguez, N. Vanthuyne, J. Crassous and L. Sánchez, *Nanoscale*, 2024, **16**, 13041.

38 G. Bringmann, T. Gulder, T. A. M. Gulder and M. Breuning, *Chem. Rev*. 2011, **111**, 563.

39 a) H. Maeda, Y. Bando, K. Shimomura, I. Yamada, M. Naito, K. Nobusawa, H. Tsumatori and T. Kawai, *J. Am. Chem. Soc*. 2011, **133**, 9266; b) E. M. Sánchez-Carnerero, F. Moreno, B. L. Maroto, A. R. Agarrabeitia, M. J. Ortiz, B. G. Vo, G. Muller and S. de La Moya, *J. Am. Chem. Soc.* 2014, **136**, 3346.

40 F. Würthner, C. R. Saha-Möller, B. Fimmel, S. Ogi, P. Leowanawat and D. Schmidt, *Chem. Rev*. 2016, **116**, 962.

41 J. Kumar, T. Nakashima, H. Tsumatori and T. Kawai, *J. Phys. Chem. Lett.* 2014, **5**, 316.

42 J. Kumar, H. Tsumatori, J. Yuasa, T. Kawai and T. Nakashima, *Angew. Chem. Int. Ed.* 2015, **54**, 5943.

43 Y. Sheng, D. Shen, W. Zhang, H. Zhang, C. Zhu and Y. Cheng, *Chem. Eur. J.* 2015, **21**, 13196.

44 D. Deb, M. Parashar, S. Sarkar, S. Ghosh, S. Balasubramanian and S. J. George, *Angew. Chem. Int. Ed.* 2025, e20385.

45 F. Lin, X. Zhang, J. Zhao, S. Shi, D. Liu, K. Wang, Z. Geng, F. Song, F. Li, and B. Z. Tang, *Angew. Chem. Int. Ed*. 2025, e15768

46 C. Du, Z. Li, X. Zhu, G. Ouyang and M. Liu, *Nat. Comm*. 2022, **17**, 1294.

47 J. Han, D. Yang, X. Jin, Y. Jiang, M. Liu and P. Duan, *Angew. Chem. Int. Ed.* 2019, **58**, 7013.

48 H. Zhang, J. Han, X. Jin and P. Duan, *Angew. Chem. Int. Ed.* 2021, **60**, 4575.

49 (a) S. Tadepalli, J. M. Slocik, M. K. Gupta, R. R. Naik and S. Singamaneni, *Chem. Rev.* 2017, **117**, 12705; (b) D.-W. Zhang, M. Li and C.-F. Chen, *Chem. Soc. Rev*. 2020, **49**, 1331

50 (a) E. Peeters, M. P. T. Christiaans, R. A. J. Janssen, H. F. M. Schoo, H. P. J. M. Dekkers and E. W. Meijer, *J. Am. Chem. Soc.* 1997, **119**, 9909; (b) Y. Geng, A. Trajkovska, S. W. Culligan, J. J. Ou, H. M. P. Chen, D. Katsis and S. H. Chen, *J. Am. Chem. Soc*. 2003, **125**, 14032.

51 (a) G. Lu, Z. -G. Wu, R. Wu, X. Cao, L. Zhou, Y.-X. Zheng and C. Yang, *Adv. Funct. Mater*. 2021, **31**, 2102898; (b) J. R. Brandt, X. Wang, Y. Yang, A. J. Campbell and M. J. Fuchter, *J. Am. Chem. Soc.* 2016, **138**, 9743.

52 Z. Geng, Z. Liu, H. Li, Y. Zhang, W. Zheng, Y. Quan and Y. Cheng, *Adv. Mater*. 2023, **35**, 2209495.

53 R. Chowdhury, M. D. Preuss, H.-H. Cho, J. J. P. Thompson, S. Sen, T. K. Baikie, P. Ghosh, Y. Boeije, X. Wei Chua, K.-W. Chang, E. Guo, J. van der Tol, B. W. L. van den Bersselaar, A. Taddeucci, N. Daub, D. M. Dekker, S. T. Keene, G. Vantomme, B. Ehrler, S. C. J. Meskers, A. Rao, B. Monserrat, E. W. Meijer and R. H. Friend, *Science*, 2025, **387**, 1175.

54 Y.-X. Yuan, J.-H. Jia, Y.-P. Song, F.-Y. Ye, Y.-S. Zheng and S.-Q. Zang, *J. Am. Chem. Soc*. 2022, **144**, 5389.

55 Y. Shi, J. Han, X. Jin, W. Miao, Y. Zhang, and P. Duan, *Adv. Sci*. 2022, **9**, 2201565.

56 S. Lin, S. Zeng, Z. Li, Q. Fan, and J. Guo, *ACS Appl. Mater. Interfaces* 2022, **14**, 30362.

View Article Online
DOI: 10.1039/D6SC00729E

Data availability

No primary research results, software or code have been included and no new data were generated or analysed as part of this review.